STRUCTURAL, OPTICAL AND ELECTRICAL CHARACTERIZATION OF CDSEXTE1-X THIN FILMS

A THESIS SUBMITTED TO
THE GRADUATE SCHOOL OF NATURAL AND APPLIED SCIENCES
OF
MIDDLE EAST TECHNICAL UNIVERSITY

BY

MERVE DEMİR

IN PARTIAL FULFILLMENT OF THE REQUIREMENTS
FOR
THE DEGREE OF MASTER OF SCIENCE
IN
PHYSICS

JANUARY 2020

Approval of the thesis:

STRUCTURAL, OPTICAL AND ELECTRICAL CHARACTERIZATION OF CDSEXTE1-X THIN FILMS

submitted by **MERVE DEMİR** in partial fulfillment of the requirements for the degree of **Master of Science** i**n Physics, Middle East Technical University** by,

Prof. Dr. Halil Kalıpçılar
Dean, Graduate School of **Natural and Applied Sciences** _____

Prof. Dr. Altuğ Özpineci
Head of the Department, **Physics** _____

Prof. Dr. Mehmet Parlak
Supervisor, **Physics, METU** _____

Prof. Dr. A. Çiğdem Erçelebi
Co-Supervisor, **Physics, METU** _____

Examining Committee Members:

Prof. Dr. Nurdan Demirci Sankır
Material Science and Nanotechnology Eng., METU _____

Prof. Dr. Mehmet Parlak
Physics, METU _____

Prof. Dr. Dilber Esra Yıldız
Physics, Hitit University _____

Assist. Prof. Dr. Emre Yüce
Physics, METU _____

Prof. Dr. A. Çiğdem Erçelebi
Physics, METU _____

Date: 08.01.2020

I hereby declare that all information in this document has been obtained and presented in accordance with academic rules and ethical conduct. I also declare that, as required by these rules and conduct, I have fully cited and referenced all material and results that are not original to this work.

Name, Last name :

Signature :

ABSTRACT

STRUCTURAL, OPTICAL AND ELECTRICAL CHARACTERIZATION OF CDSEXTE1-X THIN FILMS

Demir, Merve
Master of Science, Physics
Supervisor : Prof. Dr. Mehmet Parlak
Co-Supervisor: Prof. Dr. A. Çiğdem Erçelebi

January 2020, 79 pages

The aim of this study is to investigate the structural, optical and electrical properties of ternary $CdSe_xTe_{1-x}$ thin films.

CdTe and CdSe thin films are being used in solar cells due to their favorable direct band gaps of 1.5eV and 1.7eV, respectively. Moreover, having high absorption coefficients provide an important role to CdTe and CdSe films as an absorber layer. Therefore, by mixing these two films, properties of resultant ternary $CdSe_xTe_{1-x}$ alloy can be optimized for solar cell applications. Chemical similarities between Te and Se and the structural similarities between CdTe and CdSe provides broad range of solid solubility. By changing the ratio of Se to Te, structural, optical and electrical properties of $CdSe_xTe_{1-x}$ can be tuned and hence, promising results can be obtain for solar energy conversion technology.

Ternary $CdSe_xTe_{1-x}$ thin films deposited by stacking electron beam evaporated CdTe layers on top of thermally evaporated CdSe layers. In order to identify the effects of varying stoichiometry on structure, $CdSe_xTe_{1-x}$ films with different constituent ratios were prepared. In addition, effects of the post deposition treatment, specifically post annealing, were analyzed and the process were optimized. The structural properties

of the films were investigated by X-ray diffraction (XRD), Raman spectroscopy and energy-dispersive X-ray diffraction (EDX). For optical characterization of the films, UV-Vis spectroscopy was employed and the band gap values of $CdSe_xTe_{1-x}$ thin films were determined. Electrical characterization includes temperature dependent conductivity and photoconductivity measurements. Moreover, surface structure of the $CdSe_xTe_{1-x}$ thin films was examined by atomic force microscope (AFM) and scanning electron microscope (SEM).

It was discovered that formation of $CdSe_xTe_{1-x}$ thin films can be observed by post heat treatment at 400°C for 60 minutes. XRD and Raman spectroscopy results showed that films have polycrystalline nature and crystallinity increase with increasing annealing temperature. However, it is found that in order to preserve desired stoichiometry the upper limit should be set for annealing procedure. Otherwise, Se evaporation at high temperatures leads to variations in composition of the films uncontrollably. Furthermore, band gap of $CdSe_xTe_{1-x}$ thin films can take values between $1.4\ eV \leq E_g \leq 1.7\ eV$ and conductvity values on the order of 10^{-7} $(\Omega.cm)^{-1}$.

Keywords: CdTe, CdSe, Ternary Alloy, Thin Film

ÖZ

CDSEXTE1-X İNCE FİLMLERİN YAPISAL, OPTİK VE ELEKTRİKSEL ÖZELLİKLERİNİN KARAKTERİZASYONU

Demir, Merve
Yüksek Lisans, Fizik
Tez Yöneticisi: Prof. Dr. Mehmet Parlak
Ortak Tez Yöneticisi: Prof. Dr. A. Çiğdem Erçelebi

Ocak 2020, 79 sayfa

Bu çalışmanın amacı, üçlü $CdSe_xTe_{1-x}$ ince filmlerin yapısal, optik ve elektriksel özelliklerinin araştırılmasıdır.

CdTe ve CdSe ince filmler, sırasıyla 1.5eV ve 1.7eV'lik direkt yasak enerji bant değerleri nedeniyle güneş pillerinde kullanılmaktadır. Ek olarak, yüksek absorpsiyon katsayılarına sahip olmaları da CdTe ve CdSe filmlerinin güneş hücrelerinde emici tabaka olarak kullanılmasında önemli bir etkendir. Bu nedenle, bu iki film karıştırılarak, ortaya çıkan üçlü CdSexTe1-x alaşımının özellikleri güneş hücresi uygulamaları için optimize edilebilir. Te ve Se arasındaki kimyasal ve CdTe ve CdSe arasındaki yapısal benzerlikler geniş bir katı çözünürlüğü sağlar. Se ve Te oranını değiştirilerek, $CdSe_xTe_{1-x}$'in yapısal, optik ve elektronik özellikleri ayarlanabilir ve böylece güneş enerjisi teknolojisi için umut verici sonuçlar elde edilebilir.

CdSexTe1-x ince filmler, termal olarak buharlaştırılmış CdSe katmanlarının üzerine, elektron demeti ile buharlaştırılan CdTe katmanların istiflenmesi ile oluşturuldu. Değişken stokiyometrinin yapı üzerindeki etkilerini tanımlamak için, farklı bileşen oranlarında $CdSe_xTe_{1-x}$ filmler hazırlandı. Ek olarak, üretim sonrası ısıl tavlama

işleminin etkileri analiz edildi ve bu işlem için optimize değerler tespit edildi. Filmlerin yapısal özellikleri, X ışını kırınımı (XRD), Raman spektroskopisi ve enerji dağıtıcı X ışını kırınımı (EDX) ile incelendi. Filmlerin optik karakterizasyonu için UV-Vis spektroskopisi kullanılıp, CdSexTe1-x ince filmlerin bant aralığı değerleri belirlendi. Elektriksel karakterizasyon, sıcaklığa bağlı iletkenlik ve foto iletkenlik ölçümleri ile yapıldı. Ayrıca, $CdSe_xTe_{1-x}$ ince filmlerin yüzey yapısı, atomik kuvvet mikroskobu (AFM) ve taramalı elektron mikroskobu (SEM) ile incelendi.

Üçlü $CdSe_xTe_{1-x}$ ince filmlerin özellikleri ele alındığında, üretim sonrası ısıl işlem için uygun değerlerin 400°C'de 60 dakika olduğu ortaya kondu. XRD ve Raman spektroskopisi sonuçları, filmlerin polikristal yapıya sahip olduğunu ve tavlama sıcaklığının artmasıyla kristalliğin arttığını gösterdi. Bununla birlikte, istenen stokiyometriyi korumak adına tavlama işleminde sıcaklık için bir üst sınırın belirlenmesi gereği ortaya kondu. Aksi takdirde, yüksek sıcaklıklarda gözlenen Se buharlaşmasının filmlerin bileşiminde kontrolsüz değişiklikler oluşturabileceği gözlendi. Ayrıca, $CdSe_xTe_{1-x}$ ince filmlerin bant enerjilerinin $1.4\ eV \leq E_g \leq 1.7\ eV$ arasında değerler alabildiği ve iletkenliklerinin $10^{-7}(\Omega.cm)^{-1}$ mertebesinde olduğu ortaya kondu.

Anahtar Kelimeler: CdTe, CdSe, Üçlü Alaşım, İnce Film

ACKNOWLEDGMENTS

I would like to express my gratitude to my supervisor Prof. Dr. Mehmet Parlak for his valuable guidance through this study. It was a privilege for me to gain experimentalist insight by working with him. I would also like to present my sincere thanks to my co-supervisor Prof. Dr. Çiğdem Erçelebi for her endless support and valuable advices.

I would like to thank our group members Hasan Hüseyin Güllü, Özge Sürücü, Makbule Terlemezoğlu, Çiğdem Doğru and Tunç Bektaş for everything that they taught me. Especially, I would like to thank GÜNAM member and my dear friend Seçil Güler for her unique friendship. The technical assistance of Yücel Eke is gratefully acknowledged. I have to mention my appreciation to Gülşen Özdemir Parlak for her help on administrative matters.

With a deep sense of gratitude, I would like to express my thanks to Gökhan Alkaç for his continuous encouragement, wise advices and especially delightful friendship. It is my privilege to have a mentor like him.

My special thanks go to my dear friends Elif Ünsal, Ahmet Azgın, Ümit Doğan Dağlum and Özgür Durmuş. They never feel hesitate to help me in any issue. Also, I would like to thank Vassily Burwitz for his priceless friendship and valuable comments. I thank my cousin and my graphic designer Yaprak Deniz Yurt for her help during the thesis process and her patience.

Finally, I would like to express my deepest thanks to my family. I, as a female in the Middle East, was able to study physics thanks to my mother's encouragement. Also, I would like to express my thanks to my brother.

This work is funded by The Scientific and Technological Research Council of Turkey (TÜBİTAK) under grant number 118F317.

TABLE OF CONTENTS

LIST OF TABLES

TABLES

LIST OF FIGURES

FIGURES

CHAPTER 1

INTRODUCTION

Chalcogenide materials have gained extensive interest due to their superior properties especially in photovoltaic (PV) industry. These materials are the composition of elements from groups IIB and VIA of the periodic table. Cadmium based chalcogenides are promising materials to increase the efficiency of thin film solar cells in energy conversion technology. Among these, CdTe and CdSe are two primary chalcogenides in solar energy conversion technology due to their high absorption coefficients and direct band gap natures[1][2].

Besides energy conversion, CdTe and CdSe have wide spectrum of applications in the several branches of the technology. Numerous implementation of CdSe is present such as thin film transistors[3], photoreceptors[4], light emitting diodes[5] and solar cells[6]. Similarly, usage areas of CdTe can be count as light emitting devices and gamma detectors[7]. However, the main application area of CdTe thin films are solar cells. CdTe solar cells have the largest market share in the thin film photovoltaic industry[8].

CdTe and CdSe are two of the most studied thin films due to their wide range of applications and promising properties for the energy conversion technology. Hence, several researches were conducted to analyse properties and different deposition methods of these films. It is known that CdTe thin films can be produced by chemical molecular beam deposition[9], thermal evaporation[10], RF magnetron sputtering[11], chemical bath deposition[12], and electron beam deposition[13] etc. Likewise, CdSe has been deposited by variety of methods such as electrodeposition[2], pulsed laser deposition[14], electron beam and thermal evaporation[15] etc. Thus, multiple methods can be employed in the deposition

process and hence, qualitative CdSe and CdTe films can be deposited in a cost efficient way in large scales. Furthermore, these films have an important role on solar energy conversion technology owing to their preferable qualities. Both CdTe and CdSe have high absorption coefficient, approximately in the order of $10^5 cm^{-1}$, which is favourable for the photovoltaics[16]. In addition, having direct band gap which falls into visible range of the solar spectrum is another main advantage of CdTe and CdSe for solar cell applications[2].

Power conversion efficiency of CdTe thin film solar cells have reached 21%[17]. The most common partner of CdTe in these thin film solar cells are CdS which serves as a window layer. However, due to wide band gap of CdS (2.4 eV) photons whose wavelength in the 300-525 nm range is absorbed by CdS layer and hence cannot contribute the photocurrent of the cell[18]. Moreover, the lattice mismatch between CdTe and CdS have brought another issue. Although, the formation of CdS_xTe_{1-x} and $CdTe_yS_{1-y}$ interphases reduce the lattice mismatched, it is known that high defect density causes loss of efficiency[19]. Therefore, considering the theoretical limits for energy conversion efficiency of CdTe solar cells which is as high as 28%[20], CdSe can be proposed as an important alternative to overcome these issues originated from CdTe/CdS junction.

In order to improve the power conversion efficiency of CdTe solar cells, alloying CdSe could be suitable choice. $CdSe_xTe_{1-x}$ ternary alloy is promising material since it combines both CdSe and CdTe properties and hence make them tunable. Solid solubility of CdSe into CdTe is relatively high since the difference in lattice constants is about 6% so reduced the lattice mismatch[19]. Morover, physical and chemical similarities between Se and Te chalcogenides, specifically having the same number of valance electrons prevent the formation of dopant like defects in the $CdSe_xTe_{1-x}$ thin films[21]. It is known that physical properties of $CdSe_xTe_{1-x}$ are strictly depending on stoichiometry of the films or basically Se/Te ratio[22]. While the band gap of CdTe and CdSe thin films are 1.5 and 1.7 eV, the band gap of $CdSe_xTe_{1-x}$ alloy can take values in between 1.3-1.7eV[23]. The bowing effect in the band gap of $CdSe_xTe_{1-x}$ alloys provides to span wider range in the spectrum which increase the

solar energy harvesting. Therefore, band gap tailoring can be achieved by varying the ratios of constituent elements of $CdSe_xTe_{1-x}$. In addition, for the deposition of $CdSe_xTe_{1-x}$ thin films, various techniques were used such as molecular beam epitaxy[24], chemical bath deposition[25], hot wall deposition[23], electrodeposition[26]. Yet, by optimizing the deposition process and investigating the effects of post deposition treatments, improvements on fabrication of high quality $CdSe_xTe_{1-x}$ thin films can be achieved. Furthermore, the extensive characterization of these films may provide suitable applications which will turn as solar cells having higher power conversion efficiency.

In this study, the main object was to characterize of $CdSe_xTe_{1-x}$ thin films by means of investigating structural, optical and electrical properties of $CdSe_xTe_{1-x}$ thin films. The proposed deposition method was stacking CdTe and CdSe thin films evaporated by using e-beam and thermal evaporation techniques simultaneously. This research, also includes the analysis of the post heat treatment effects on the properties of $CdSe_xTe_{1-x}$ thin films. The structure of this study; in Chapter 2, brief information on semiconductors and its properties were presented. After discussing theoretical background of some characteristic properties of semiconductors, detailed information on group II-VI semiconductors, namely properties of CdTe and CdSe thin films were introduced. In Chapter 3, the experimental instrumentation that employed in this study was introduced with their working principles. In Chapter 4, the results of the characterization studies were explained. In Chapter 5, conclusions of this study were summarized.

CHAPTER 2

THEORETICAL BACKGROUND

2.1 Introduction

In this section brief information on semiconductors, namely types, origins of optical and electronic properties were presented. The transmission and the conduction mechanisms were discussed with the theory behind the experiments. Following, chalcogenides were introduced. In this part, physical properties of chalcogenides were mentioned and reasons of being significant component of photovoltaic industry were summarized. Lastly, CdTe and CdSe which are the two popular binary compounds in chalcogenides, were discussed as the main interest of this thesis.

2.2 Fundamentals of Semiconductors

Semiconductor materials are taking interest since 1870s with the discovery of the photoconductive behavior of selenium[27]. Until then there are numerous breakthrough inventions and application areas such as transistors[28], photodiodes[27] and solar cells are developed. CdSe and CdTe are the most widely studied and used semiconductors in technology.

Semiconductors are described by their energy band structures. These energy bands are separated from each other with regions called energy gap or band gap. When external electric field is applied, the response of the material shows significant differences related with the occupancy of the energy bands. If the allowed energy bands are fully filled or empty, electrons would not move with the electric field so the material is called as insulator. If the energy bands are occupied partially, electrons move with electric field and these materials are called as conductors. Also, there is a middle case of insulators and conductors which are semiconductors. In

semiconductors, slightly filled or empty energy bands provide freedom to move to electrons regarding external conditions such as temperature[29].

The electronic states of an isolated atom are discrete such as energy levels of isolated hydrogen atom. However, when two identical hydrogen atoms brought closer, splitting of energy levels is observed. The reason of this splitting can be explained by Pauli exclusion principle which state that for a given system two electrons cannot reside in the same energy level at the same time[30]. Considering system having N number of atoms, these splitting of energy levels occurs as much as the number of atoms. As the number of atoms increases the number of discrete energy levels also increase but separate levels get close to each other. When N is large as in solids, the resultant state for an electron is continuous band of energy.

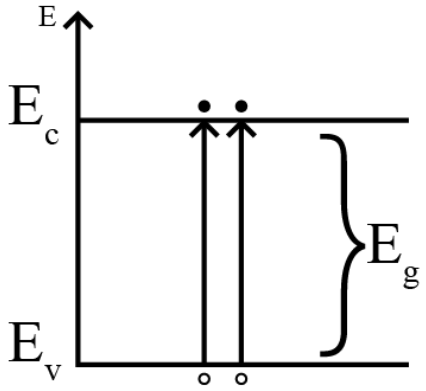

Figure 2-1. Energy diagram of semiconductors

Nature of the band structures is characteristic of solids. At temperature absolute zero, all electrons occupy the states that has the lowest energy. This lower band that is occupied by electrons at 0K is called valance band while the upper one is called conduction band. As illustrated in Fig. 2.1, the top of the valance band is denoted by E_v and the bottom of the conduction band is denoted by E_c. The distance between E_v and E_c is called bandgap energy, E_g. There are no allowed energy states are present in the gap so it is sometimes called forbidden band[31].

At low temperatures, electronic states in the valance band are fully filled with electrons while states in the conduction band are empty. Because of this,

semiconductors behave as insulators at low temperatures. However, since the band gap values of semiconductors are in the order of a few eV, thermal energy is sufficient to excite electrons in the valance band to the conduction band at high temperatures[32]. By gaining thermal energy, electrons move to conduction band and leave equal number of positively charged holes in the valance band. These types of semiconductors are referred as intrinsic semiconductors. If a semiconductor is doped with impurity atoms additional energy levels originated from impurities are introduced and semiconductor is called extrinsic[30]. If the impurity atoms have extra electron with small binding energy to the host atom, this electron is donated to the conduction band. In this situation impurity atom is called donor and semiconductor becomes n-type due to excess of electron. In the other case, impurity atom accepts extra electron and leave positively charged hole in the conduction band. This creates p-type semiconductor and impurities are called acceptor.

Addition of impurities brake the periodicity of the lattice and causes imperfections in the structure. Hence, with these impurities, additional energy levels are introduced in the band gap. Therefore, forbidden states in the band gap are become possible energy levels. Illustration of intrinsic and extrinsic semiconductor band diagrams are given in Fig. 2.2.

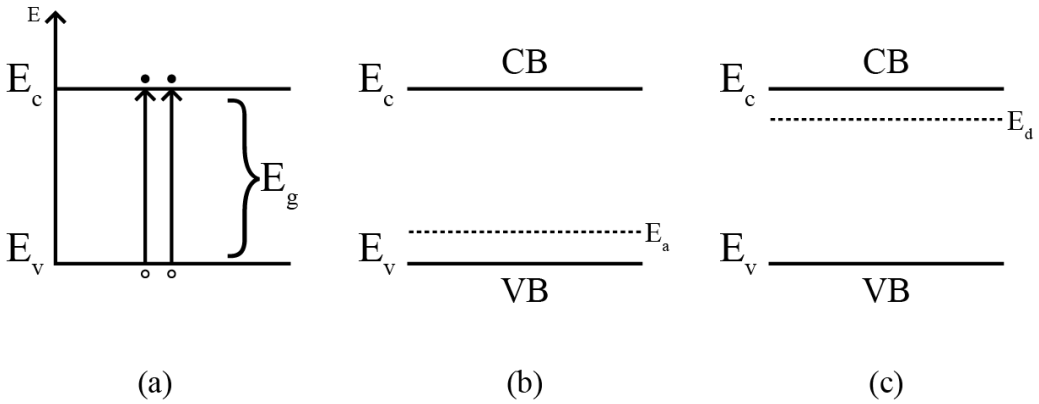

Figure 2-2. Types of semiconductors; (a) intrinsic, (b) p-type, (c) n-type

2.2.1 Optical Properties of Semiconductors

Optical properties of semiconductors are defined with the results of the interaction between material and electromagnetic radiation. The perturbation of the electromagnetic field on semiconductor can results in transitions between electronic states or the vibrational states or both. Hence, optical studies give important insight about lattice vibrations of the material. Moreover, due to close relationship between incident radiation and energy states, band gap of semiconductors can be determined by optical measurements.

2.2.1.1 Transmission

In optical characterization of materials two important quantities, transmittance and reflectance are generally measured. Transmittance T of a sample with light incident normal to the surface is given by,

$$T = \frac{(1-R)^2 e^{-\alpha d}}{1 + R^2 e^{-2\alpha d} - 2Re^{-\alpha d} cos\phi} \tag{2.1}$$

where d is the thickness of the sample, in Eq.2.1 $\phi = 4\pi nd/\lambda$ where λ is the wavelength of the incident radiation, n is called index of refraction and usually depends on frequency. Absorption coefficient is defined as,

$$\alpha = \frac{4\pi k}{\lambda} \tag{2.2}$$

where k is the extinction coefficient and reflectance R is,

$$R = \frac{(n_0 - n)^2 + k^2}{(n_0 + n)^2 + k^2} \tag{2.3}$$

where n_0 is the index of refraction of the ambient medium. As mentioned previous section, band structure of semiconductors has significant impact on optical properties. If the incident photon has energy less than the band gap value, the semiconductor is transparent and hence α≈0 so that Eq.2.1 becomes,

$$T = \frac{(1-R)^2}{1+R^2-2Rcos\phi} \tag{2.4}$$

The cosine term in above equation is related with characteristic spatial frequency and resolution power of the instrumentation of optical systems can be insufficient to measure its contribution[33] therefore, Eq. 2.4 becomes,

$$T = \frac{(1-R)^2}{1-R^2} = \frac{1-R}{1+R} \tag{2.5}$$

However, impurities in a material have a role on absorption of incident photons. Since density of impurities is proportional to α, transmittance formula with absorption is,

$$T = \frac{(1-R)^2 e^{-\alpha d}}{1-R^2 e^{-2\alpha d}} \tag{2.6}$$

Hence, α can be written in form,

$$\alpha = -\frac{1}{d} ln \left[\frac{\sqrt{(1-R)^4 + 4T^2R^2} - (1-R)^2}{2TR^2} \right] \tag{2.7}$$

For semiconductors, having high absorption coefficient such as CdTe and CdSe, the reflectivity takes negligible values. Moreover, the effects originated from interference can be ignored. Therefore, with simplification α can be expressed as,

$$\alpha = -\frac{1}{d} \ln(T) \tag{2.8}$$

Figure 2-3 shows possible transitions of electrons due to absorption of photon. The relation between absorption and band gap is,

$$\alpha \sim \left(h\nu - E_g\right)^{\gamma} \tag{2.9}$$

where hν is the energy of incident photon. Constant γ can take values according to nature of transitions.

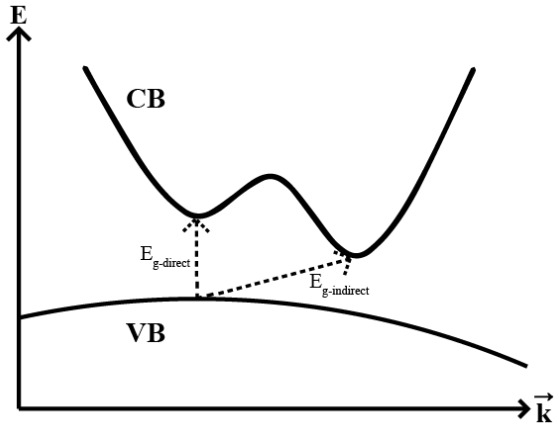

Figure 2-3. Direct and indirect transitions of electrons

In Fig. 2.3 direct and indirect transitions is illustrated. γ equals to ½ for allowed direct transition in which bottom of the conduction and top of the valance band have the same wave vector value, $k_{max}=k_{min}$ hence, transition occurs vertically. γ equals to 2 for allowed indirect transition where k points of conduction and valance bands extrema have different values and phonons included in order to conserve momentum. For direct band gap semiconductors $(\alpha h\nu)^2$ vs hν graph, for indirect band gap semiconductors $(\alpha h\nu)^{1/2}$ vs hν graph is plotted. Extrapolated intercept of the energy axis of these graphs gives band gap value of semiconductor. These graphs are called Tauc plots[33].

2.2.2 Electrical Properties of Semiconductors

2.2.2.1 Resistivity

The resistivity of a semiconductor is an important parameter since it contributes device series resistance or capacitance. Resistivity, ρ is defined as,

$$E = \rho J \tag{2.10}$$

where E is the electric field and J is the current density. Moreover, reciprocal of ρ is defined as conductivity, $\sigma=1/\rho$ and,

$$J = \sigma E \tag{2.11}$$

For semiconductors, carrier densities both electrons (n) and holes (p) and electron and hole mobilities μ_e and μ_p construct ρ as,

$$\rho = \frac{1}{q(\mu_n n + \mu_p p)} \tag{2.12}$$

However, in general carrier densities and mobilities are unknown[33]. Therefore, common techniques for measuring resistivity are two-point or four-point probe methods. Two-point probe method provides ease of use, however; analysis of data can be more complex since each probe serves as both current and voltage probes. Derivation of resistivity starts with,

$$E = \rho J = -\frac{dV}{dr} \tag{2.13}$$

By inserting J= $\frac{I}{2\pi r^2}$ we get,

$$V = -\frac{I\rho}{2\pi}\int_0^r \frac{dr}{r^2} = \frac{I\rho}{2\pi r} \tag{2.14}$$

Since current flow area on the sample and probe spacing, s, is comparable resistivity become,

$$\rho = \frac{2\pi s V}{I} \tag{2.15}$$

However, due to sample shape, correction factors, F, should be included so,

$$\rho = 2\pi s F \frac{V}{I} \tag{2.16}$$

With these correction factors, geometrical aspects of the samples such as thickness, lateral dimensions and edge effects can be taken into account. Thickness correction F_1 is given by[33],

$$F_1 = (t / s)/(2\ln\{(\sinh(t / s)/(\sinh(t / 2s)\}\}) \tag{2.17}$$

where t is the thickness of the sample. For thin samples $\sinh(x) \approx x$ for $x \ll 1$ approximation can be done so that ρ becomes,

$$\rho = \frac{\pi}{\ln(2)} t \frac{V}{I} \tag{2.18}$$

Moreover, sheet resistance, R_{sh}, is an important parameter for thin layers and given by,

$$R_{sh} = \frac{\rho}{t} = \frac{\pi}{ln2} \frac{V}{I} \tag{2.19}$$

2.2.3 Optoelectronic Properties of Semiconductors

2.2.3.1 Photoconductivity

Photoconductivity is based on absorption of photon which causes the production of free carriers. For semiconductors that show photoconductive effect, the conductance can be changed by the energy of incident photons. If the energy of incident photon is sufficient, it can excite the electron in the valance band to the conduction band which referred as intrinsic photoconductivity. Ionization by photon can be occur also from donor, acceptor or other impurity levels then, it is called impurity photoconduction[34]. The schematic representation of photoconductivity and energy levels are shown in Fig.2.4. Conductivity that depends on electrons and holes without illumination at specific temperature is called dark conductivity. In the theory developed by Mott and Davis conductivity is in the form[35],

$$\sigma = \sigma_0 \exp(-E_a/kT) \tag{2.20}$$

where $E_a$is the activation energy. This temperature dependence of conductivity can be applied both amorphous and crystalline semiconductors. In several research, temperature range between $180K < E_a < 220K$ single activation energy was reported[35].

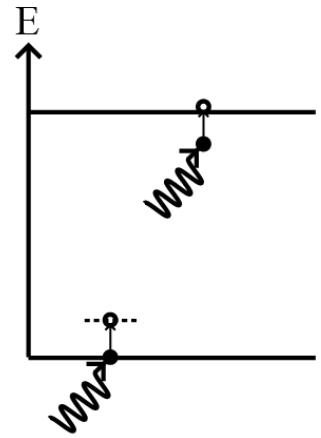

Figure 2-4. Impurity photoconduction

For semiconductors whose free carrier concentration is low or semiconductors at low temperatures, conductivity can be enhanced by electromagnetic radiation in which photon energies are equal or greater than the band gap, i.e. $h\upsilon \geq E_g$. At higher temperatures, change in conductivity due to photons has relatively small effect. However, still it can be managed by sending photons with high intensity in other words incident radiation with high power per unit area of illumination[32].

2.3 Group II-VI Semiconductors; Chalcogenides

The elements of the group sixteen in periodic table are named as chalcogens and the compounds contain one of these elements are referred as chalcogenides. Binary compounds of elements from group IIB and group VIA are common chalcogenides and called II-VI compounds.

II-VI compounds crystallize in both cubic zinc-blend (sphalerite) or hexagonal wurtzite (zincite) structures[36]. Varying preferred orientation is highly related with the deposition conditions, mainly the temperature[37]. It is also known that these binary compounds can undergo solid-solid transition resulting phase changes under their melting points[38]. Furthermore, II-VI compounds can show either p-type or n-type conductivities. Some of them can be prepared with both p- and n-type forms like CdTe and ZnSe by arranging deposition techniques and parameters[4]. Group II-VI compounds have wide range application areas such as photodetectors, light-

emitting diodes(LEDs), biophotonics and specifically solar cells[39]. The main reasons why cadmium chalcogenides are proper candidates for photovoltaics can be listed as,

- Their direct band gap, nearly 1.5eV, provides advantage for harvesting solar energy.
- High optical absorption coefficients, nearly $10^4 cm^{-1}$, make them suitable for manufacturing optical devices in thin film form[37].
- Stable compounds can be manufactured with several different methods[8]

Hence, chalcogenides are gain attention due to their superior properties. Cadmium chalcogenides such as Cadmium Telluride (CdTe) and Cadmium Selenide (CdSe) are considered as important components of the thin film cells. Therefore, these chalcogenides are the most widely studied and promising materials for solar cell technology[4].

2.3.1 Thin Film Chalcogenides

Chalcogenides in the thin film form are one of the primary components of the solar cell technology. The material properties of the chalcogenides thin films, such as the main object of this thesis CdTe and CdSe, is strongly depends on the deposition technique. Therefore, particular deposition methods result in qualitative chalcogenide thin films with desired functions. Thin films are different from bulk structures with their thickness and structure. These are the layers of material having thickness between nanometers to several micrometers. Thin films can be deposited in both liquid and vapor phases. However, vapor phase deposition techniques have more advantages such as being more applicable or providing more controllable processes[40]. Common vapor phase fabrications include physical vapor deposition (PVD) and chemical vapor deposition (CVD). For chalcogenide thin films, phase transition from amorphous to crystal can be observed related with the deposition method[41]. Therefore, chalcogenide thin films can be manufactured in amorphous or crystalline forms. These crystalline structures can be periodic for whole range

which results in single crystal thin films. However, highly related with varying deposition techniques, the ideal arrangement of the atoms may differ. As a consequence, the different sizes of the crystallites, in other words grains can be obtained. In that case, the films are composed of small crystallites generally having sizes between 1-100 nm and they are called polycrystalline. In the application of polycrystalline semiconducting thin films, the grains sizes and grain boundaries are determinative on optical and electrical properties.

2.3.2 Binary II-VI Compounds; Properties of CdTe and CdSe

CdTe thin films are crystallized in zinc blend structure. This structure composed of two face centered cubic (FCC) into each other by ¼ of the cube diagonal along [111] direction. One of these two FCC structures form of cations while the other one form of anions[42]. Since it is in cubic form only one parameter, lattice distance a, is sufficient to define unit cell of the structure. Moreover, it is composed of four molecules and each atom tetrahedrally bonded to the nearest neighbor atom. On the other hand, both zinc blende and wurtzite structure are observed for CdSe thin films in literature. Wurtzite structure is close to zinc blend in terms of bonding of atoms. Unit cells are composed of two molecules of compounds but again four atoms each bonded tetrahedrally to the neighbors[42]. The main difference is, instead of face center cubic, the hexagonal closed packed (HCP) lattice is formed. To describe wurtzite crystal structure two parameters should be known: the hexagon height c, and the edge length a. Also, c/a ratio is used and ideally this ratio is $c/a=(8/3)^{1/2}=1.633$. However, it is common some deviations occur in this ratio due to anion cation distance along c-direction can be slightly different from in other directions[39].

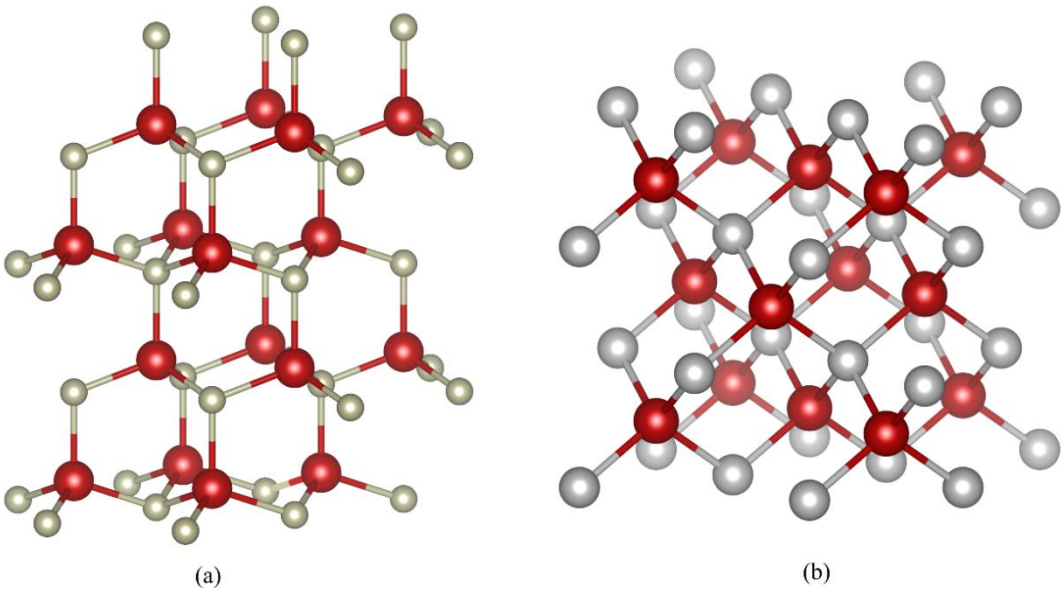

Figure 2-5. Crystal structures of (a) Wurtzite-CdSe, (b) Zinc-blende CdTe

The crystal structures of zinc blende CdTe and wurtzite CdSe are presented in Fig. 2.5. The lattice constants of cubic CdTe and cubic CdSe are given a=6.481 Å and a=6.077 Å in International Center for Diffraction Database (ICDD) with card number 15-0770 and 19-0191, respectively. The interplanar distances of the CdTe and CdSe in [111] direction are d=3.742 Å and d=3.510 Å in ICDD, respectively.

The structural, optical and electrical properties of CdTe were investigated with varying conditions such as deposition technique[43], thickness[44] or Cd/Te ratios[9]. It is known that CdTe thin films have direct band gap with band energy value 1.5eV. Small deviations in band gap with varying deposition methods or post deposition treatments were observed. Likewise, the resistivity of CdTe films can take varying values in the order of 10^3-10^8 (Ω.cm)[9]. The Raman spectroscopy results of CdTe showed that transverse and longitudinal phonon modes occurred at 140 and 165 cm^{-1}[7]. In addition, Te phonon modes near 120 cm^{-1} can be observed in Raman spectrum of CdTe[45].

The characterization of the CdSe thin films had revealed that, similar to CdTe, CdSe thin films have direct band gap nature with 1.7eV band gap. Phonon modes of CdSe films found at 208 and 413cm^{-1} corresponds to first and second order longitudinal

modes in Raman spectroscopy[46]. Resistivity of CdSe films take values in the range 10^4-10^6(Ω.cm)[46][47]. Resistivity of the CdSe thin films can be manipulated by post treatments such as annealing. The main mechanism of the varying conductivity is proposed as the change in grain sizes which define the grain boundary effects[47]. Moreover, the same explanation has been proposed for the performance of the CdTe thin films[48].

CHAPTER 3

EXPERIMENTAL PROCEDURE

3.1 Introduction

In this chapter, experimental techniques and instrumentations that were employed to fabricate and characterize $CdSe_xTe_{1-x}$ thin films are presented in detail. First, the deposition process includes substrate preparation and growth procedure is explained. Then, structural, optical and electrical characterization methods are discussed.

3.2 Deposition of $CdSe_xTe_{1-x}$ Thin Films

3.2.1 Substrate Preparation

All $CdSe_xTe_{1-x}$ films were deposited on 1 mm soda-lime glass substrates which are manufactured by Merienfeld. For each characterization process different sizes of glass substrates, according to sample holder limits of the characterization instruments, were cut off. Glasses with sizes 1x1cm for SEM, EDX, AFM measurements and 2x2cm for XRD, Raman spectroscopy, optical measurements used as a substrate. For electronic measurements, samples were prepared with Van der Pauw geometry using cloverleaf masks shown in Fig. 3.1. Van der Pauw geometry allows to eliminate correction factors caused by width or distance differences while performing current-voltage (I-V) experiments.

Figure 3-1. Cloverleaf mask geometry

The quality of the films is highly related with being non-contaminated or not including pinholes over the surface. Therefore, appropriate cleaning procedure for the glass substrates is crucial for thin film growth. In this work, glass substrates were cleaned chemically by employing ultrasonic cleaner. After wiped with acetone as a first step of cleaning, glasses were put into ultrasonic cleaner with hot distilled water to be rinsed. In following step, hot detergent solution was used to remove the surface contaminants and rinsing with hot distilled water was repeated. To avoid any residues of detergent and the other contaminations, slides were cleaned with pure acetone and then isopropanol in ultrasonic cleaner for a period of 20 min each. In order to eliminate organic contaminants, glass slides were put into 30% hydrogen peroxide (H_2O_2) solution in ultrasonic cleaner and rinsed with hot distilled water. All cleaned glass substrates were stored in pure methanol until growth process.

3.2.1.1 Growth Process of $CdSe_xTe_{1-x}$ Thin Films

The physical vapor deposition (PVD) is a common method to fabricate thin films due to ease of use and it provides controllable process. The evaporation system that is used in this study is shown in Fig. 3.2. This system includes two different deposition sources, one is for thermal evaporation and the other is for the electron beam evaporation which can be employed simultaneously. In this study, CdTe thin film layers were deposited by electron beam evaporation while CdSe thin films were synthesized by thermal evaporation.

Figure 3-2. Thermal and e-beam evaporation system

The ternary $CdSe_xTe_{1-x}$ alloys were fabricated by stacking CdTe and CdSe layers evaporated from two different sources both having purity 99.99% (Alfa Aesar) on the well cleaned soda lime glass. By stacking thermally evaporated CdSe layers on top of e-beam evaporated CdTe layers, $CdSe_xTe_{1-x}$ thin films were synthesized as 12 layers of CdTe and CdSe, 6 layers of each. Since the main object of this study is to investigate the stoichiometric composition effects on the structure of the films, thickness of CdTe and CdSe layers were changed in between 25- 60 nm for each deposition and hence, variation in Se/Te ratio was observed.

The schematic representation of the vacuum system with both thermal and electron beam sources that used in this study is given in Fig. 3.3. This system consists of mechanical pump, turbo-molecular pump, stainless steel vacuum chamber, base with rubber o-ring, deposition sources and substrate holder.

The growth process began by placing the substrates in the vacuum chamber with a holding plate arranged 15 cm above the deposition sources. Source pellets of CdTe

and CdSe were placed in a graphite crucible and a tungsten boat for e-beam and thermal evaporation, respectively. The shutter was placed in between source and substrates to avoid undesired deposition until controlled growth starts. Moreover, the deposition rate and thickness of the films were observed by attached Inficon XTM/2 deposition monitor during growth process. Deposition of CdSe, CdTe and $CdSe_xTe_{1-x}$ films took place at room temperature under a base pressure of approximately $1x10^{-5}$ Torr. To reach that pressure, Varian 3117 vacuum system was employed first, up to pressure 10^{-2} Torr. Then, Laybold turbo-molecular pump system was run and necessary vacuum condition for growth was achieved.

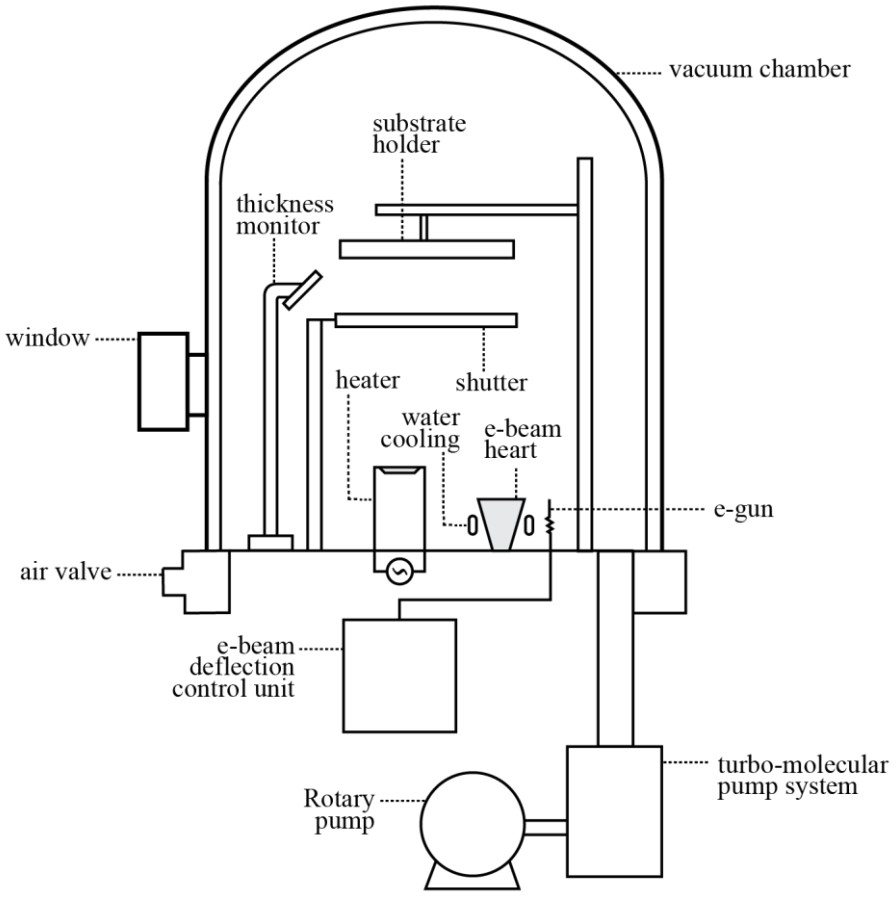

Figure 3-3. Schematic representation of thermal and e-beam evaporation system

The first layer of $CdSe_xTe_{1-x}$ films was e-beam evaporated CdTe layers to the glass substrates, so that power supply of the e-beam source was turned on as a first step. The main principle of production of electron beam is to apply current to source filament which results in electron emission. These energetic beams of electrons are sent to source material directly. As a result, evaporation occurs only in small localized area which provides both deposition of large range of materials and elimination of potential contaminations[35]. Furthermore, the direction of the accelerated electrons is controlled by electromagnets. With this feature of the system, electron beam was focused on the source material with adjusted intensity by intensity control unit. When CdTe pellets began to evaporate, stainless steel shutter between source material and substrate was removed. The deposition rate was kept approximately 4-6 Å/s which was measured by the deposition monitor. As the desired thickness of the films was reached the shutter was placed in front of substrates and the power supply of e-beam evaporator was turned off.

Following layer, on CdTe, were CdSe thin film which was deposited by thermal evaporation source. Since the system has both e-beam and thermal evaporation sources stacking of CdTe and CdSe thin films were deposited successively and repeatedly in the same system. Hence, the conditions such as growth temperature and vacuum were the same with e-beam deposition mentioned above. For growth of CdSe layers, direct thermal heating of CdSe source was done by applying voltage difference to the edges of boat. Since temperature of the source material is controlled via electrical current it is easy to manage deposition rate in thermal evaporation. Moreover, simplicity and low cost implementation are the advantages of this method[35]. The source was heated by giving AC voltage slowly. At 60V, evaporation was observed via thickness monitor, therefore, shutter was removed. The deposition rate was kept approximately 2 Å/s. When the desired thickness was reached shutter was closed and voltage was decreased slowly.

Stacking process was completed by employing e-beam and thermal evaporation techniques one by one. When deposition of the films was completed, turbo and

mechanical pumps were switched off, respectively. At each step sufficient amount of time was waited in order to break the vacuum without causing oxidation.

3.3 The Post Annealing Process

Thermal annealing is widely used method to alter intrinsic stress or improve inner structure and surface properties of the thin films[49]. In this work, thermal annealing effects as post deposition treatment on the films were investigated. Besides as deposited ones, samples annealed at different temperatures for different time durations were examined.

Annealing procedure was carried out in horizontal Lindberg type furnace as shown in Fig. 3.4. Constant nitrogen (N_2) gas flow is provided during the process to prevent any contamination from environment. Samples were placed into center of the furnace after desired temperature was reached. At the end of the planned annealing time interval, nitrogen was allowed to flow while the samples slowly cooled to room temperature.

Figure 3-4. Annealing furnace

As one of the main topics of this study, the optimization of annealing parameters such as temperature and time, these parameters varies slightly for each deposition. All metal coated films were annealed at 100°C for 30 minutes in order to get qualitative contacts between metal and the film layers. Binary CdTe and CdSe films were annealed at 200, 300 and 400℃ for 30 minutes. At first, ternary $CdSe_{0.5}Te_{0.5}$

thin films annealed at 200, 300, 400 and 450℃ for 30 minutes. After elimination of some parameters according to outcomes, remaining ternary alloy thin films were annealed at 300, 350 and 400℃ for 60 minutes.

3.4 Characterization of $CdSe_xTe_{1-x}$ Thin Films

3.4.1 Structure and Surface Analysis

3.4.1.1 X-Ray Diffraction

X-ray diffraction (XRD) is one of the most powerful characterization techniques in material sciences. With XRD measurements the crystal structures, preferred orientations of the lattice planes, inner stress and strain values can be obtained.

In crystals, atoms or molecules are present in a periodic arrangement which act as diffraction centers. Direction of the diffracted X-rays are determined according to shape and size of the unit cells[50]. Therefore, by measuring diffracted wave directions unit cell information of the unknown crystals can be extracted. The geometry of the X-ray diffraction is given in Fig. 3.5.

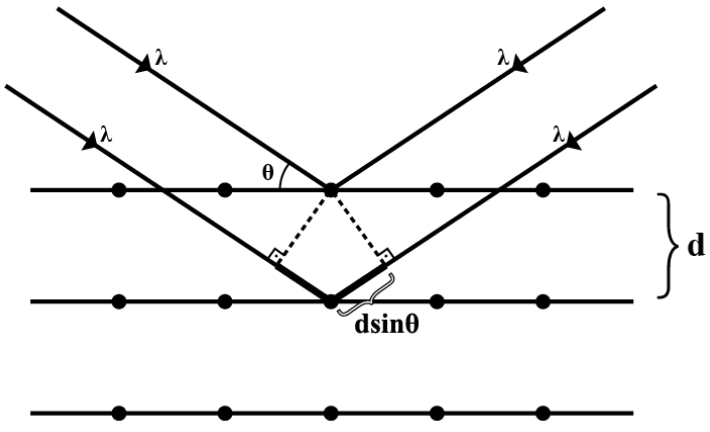

Figure 3-5. Schematic representation of X-ray diffraction

The path difference between diffracted waves leads to phase difference. This phase difference is the reason of the changings in amplitude of the wave. Hence, diffracted waves go under either constructive or destructive interference. If the path difference of the diffracted waves is equal to integer multiple of wavelength, the constructive interference occurs which is formulated by Bragg's law.

$$n\lambda = 2dsin\theta \tag{3.1}$$

By rearranging above formula and inserting the minimum possible value for n, n=1,

$$\frac{n\lambda}{2d} = sin\theta \leq 1 \tag{3.2}$$

$$\lambda \leq 2d$$

where λ is the wavelength of the X-rays, Θ is the angle of incidence, d is the interplanar distance of the crystal and it should be comparable with the incident wavelength according to above equation. As repetition of the atoms in the lattice are in the units of 1-2 Å, X-rays are the main candidate to observe diffraction patterns due to their wavelength which taking values between 1-100 Å. In addition, the angle between transmitted and diffracted wave, that is 2θ, is called diffraction angle and this angle is measured in XRD experiments.

Periodicity of the crystals not only provides constructive interference, but also destructive interference occurs. Therefore, ideally, for perfect crystals diffracted beams which are out of phase cancel each other. However, for real crystals there are imperfections and also long range periodicity is broken which define particle sizes[50]. Due to these reasons, destructive interference includes particle size information and can be calculated by XRD results by Scherer's formula.

$$D = \frac{K\,\lambda}{\beta_{2\theta}\,cos\theta} \tag{3.3}$$

where D is the crystallite size calculated from XRD results. K is Scherer constant which takes values between $0.89 \leq K \leq 0.94$ depending on the function that is used to fit peak and $\beta_{2\theta}$ is the full width half maxima (FWHM) of the peak in radians[51].

X-rays are generated by electron transitions between energy levels and hence, they are characteristic for atoms. Most common sources for X-rays are copper, molybdenum, cobalt, iron and silver for laboratory usage[52]. Electron transitions to the innermost orbitals end up emission of X-rays. For instance, transferring of the electrons from L shells to K shell will result in Kα radiation[52].

In this work, diffraction studies were carried out by Rigaku Miniflex X-ray diffraction (XRD) system equipped with CuKα radiation source with wavelength 1.54 Å. With rotating crystal method where wavelength is kept constant but angle of incidence changes, samples were examined in the 2θ range between 10° and 90° with scan speed of 4 degree/min.

3.4.1.2 Raman Spectroscopy

Raman spectroscopy is based on interaction between matter and electromagnetic radiation. The inelastic collisions of the photon and molecular vibrations result in Raman Scattering. The energy is transferred from incident radiations to molecules. As quantum mechanics proposed, this transfer mechanism work via energy packets as stated in Eq. (3.4)

$$E = h\nu = \frac{hc}{\lambda} = hck \tag{3.4}$$

where h is the Planck constant, c is the speed of light and k is called wavevector or wavenumber. Thus, the transferred energy in Raman scattering can be displayed by wavevector k.

Molecules in electric field, which can be provided by laser beam such in Raman spectroscopy, are polarized since positively charged nuclei attracted toward negative pole while electrons attracted by positive pole[53]. The result of the charge separation is the induced dipole moment P given by Eq. (3.5)

$$P = \alpha E \tag{3.5}$$

where E is electric field strength and α is a tensor of polarizability. Polarizability tensor is dependent on the shape and dimensions of the chemical bond. Since chemical bonds changes with vibration polarizability depends on vibrations[54]. If polarizability tensor changes with vibration the state is called Raman active[53].

In Fig. 3.6, types of scatterings are illustrated. If the frequency of the incident light, ν_0 is the same with the scattered light the process is called Rayleigh scattering. On the other hand, in Raman scattering the frequency of the scattered light is shifted like $\nu_0 \pm \nu_{vib}$, where ν_{vib} is the vibrational frequency of a molecule. $\nu_0 - \nu_{vib}$ lines are called Stokes scattering while $\nu_0 + \nu_{vib}$ are called anti-Stokes scattering. Therefore, frequency shift between incident and scattered radiation is measured in Raman spectroscopy.

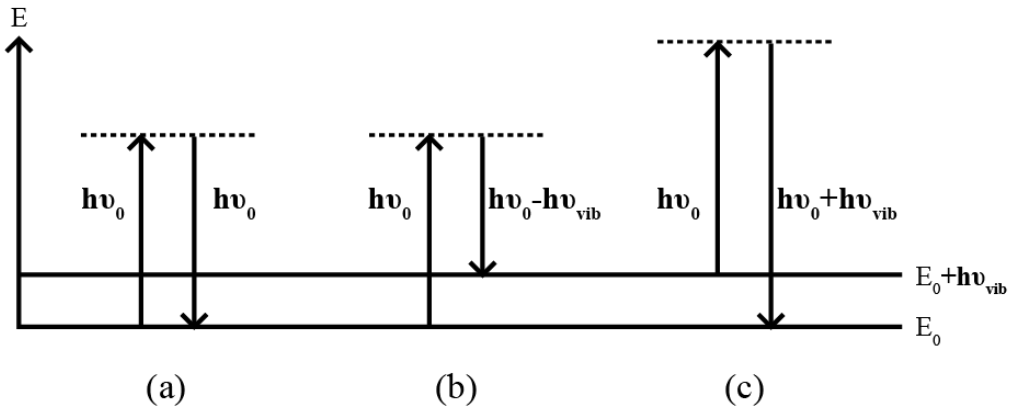

Figure 3-6. Energy transition diagram (a) Rayleigh scattering, (b) Stokes scattering, (c) anti-Stokes scattering

Molecules, that are in excited states, interact with incident photon in anti-Stokes scattering. However, most molecules are in the ground state at room temperature. This leads to having weaker anti-stokes lines rather than Stokes lines in the whole Raman spectrum. Generally, in Raman spectroscopy stokes lines are measured[55].

By using Raman spectroscopy, information on chemical bond length and angles of the molecules can be extracted since they rely on vibrational degrees of freedom. In

addition, slight band shifts in the spectrum indicate whether a compound retains its structure in different phases or physical states[55].

Figure 3-7. Raman spectroscopy setup

In this study, for Raman spectroscopy, Horiba-Jobin Yvon iHR550 imaging spectrometer shown in Fig. 3.7 with monochromator which includes three different gratings were employed. The grating was kept at 1800 grooves/mm for all samples. Optical microscope of the system includes continuous white light by halogen bulb provided by Euromex fiber optic light source. The excitation source of the system is Ventus532 laser having 532 nm wavelength designed by Laser Quantum for the Raman spectroscopy applications. Samples growth on 2x2 cm soda lime glass substrates were examined in Raman spectroscopy. Raman scatterings of each sample were measured from two different locations to confirm the homogeneity of the films.

3.4.1.3 Atomic Force Microscopy (AFM)

Atomic force microscopy (AFM) is a surface scanning method that used for extract surface topography information of the samples. In this technique nano-forces between microscope tip and the sample surface is measured and qualitative images of the surface are created. The forces, that result of interaction of the tip and the sample, can be stated as covalent, ionic or metallic bonding, Van Der Walls bonding and hydrogen bonding forces[56]. Measurement of these small forces is achieved by monitoring motion of the very flexible and ultra-light cantilever beam. Interaction force between tip and the sample causes the deflection of cantilever in which displacement is smaller than 0.1nm. Detection of this deflection can be measured by sensors that have wide range of working principles such as capacitance detection, piezoelectric detection, optical interferometry, optical laser beam detection[57].

Figure 3-8. Atomic force microscope

There are three operation modes are present for AFM. In contact mode, the tip slides across the sample surface and gather topographical data. Although it is an effective operation mode the dragging motion might be harmful for both sample and tip. In non-contact mode, the van der Walls attractive forces between sample and the tip are measured. However, these forces are weaker in comparison with the ones in contact mode, thus the resolution of the images are lower. In tapping mode, the oscillation

of the cantilever provides both high resolution due to instant contacts with surface and elimination of the dragging motion over the surface[33].

In this study, atomic force microscope measurements were done at METU Central Laboratory. AFM studies were carried out via Veeco MultiMode V AFM shown in Fig. 3.8. Samples are examined by tapping mode and both 2 and 3-D images of the surfaces were taken. Average roughness values were taken in 5μm X 5μm area.

3.4.1.4 Scanning Electron Microscopy

Scanning electron microscopy (SEM) is a widely used instrument to analyze the microstructural characteristic of the materials. In SEM, examined samples are irradiated by focused electron beam and outcome of interaction between incident electrons and material is analyzed. These interactions lead to creation of backscattered electrons, secondary electrons, characteristic X-rays and photons of various energies which they used as signals of SEM[58].

Backscattered electrons (BSE) and secondary electrons (SE) are major signals to form an image of the sample. Accelerated electrons either scattered elastically by interact with atomic nuclei or inelastically by interact with atomic electrons. If the deflection angle is less than 90° forward scattering occurs. If the deflection angle is greater than 90° the outcome is observed as BSE. Since energy loss of these electrons are small they have high kinetic energy to leave the sample and collected as BSE signal[59]. Secondary electrons are originated from outer shells electrons of the atoms which are excited by incident electron beam. Since they are poorly bounded, electrons are ejected from atoms and collected as SE[58].

The instrumentation of the electron microscope includes electron source, condenser lens system which are strong magnetic lenses, apertures to control the diameter of the electron beam, objective that is the closest magnetic lens to specimen and the detector. Electron gun of the SEM can be tungsten filament, LaB_6 emitter or a tungsten field-emission tip[59]. Parameters such as electron-accelerating voltage

which determines the kinetic energy of the primary electrons, the distance of the sample and objective lenses which is known as working distance (WD) can be controlled during SEM measurements[59]. These parameters influence the performance of the SEM.

In this study, specimens were examined by SEM in both METU central laboratory and GÜNAM. Morphology and constituents were determined by Quanta 400 FEG model Scanning Electron Microscopy (SEM) equipped with energy dispersive X-ray spectroscopy analysis system (EDAX). Before imaging with SEM, thin layer of Au (≈3nm) was deposited on all samples to overcome charging problems.

3.4.1.5 Energy Dispersive X-ray Spectroscopy (EDS)

As mentioned in previous part, compositional information of the specimens was obtained by SEM equipped with energy dispersive X-ray spectroscopy (EDS) system. The characteristic X-rays emitted as a result of electron beam-specimen interaction is collected to analyze distribution of the constituents. X-ray detectors that are attached to SEM are based on lithium drifted silicon [Si(Li)]. The characteristic X-rays of all elements above atomic number 4 can be measured by energy dispersive spectrometer[58]. Since position of the energy peak is very crucial for analyzing the present elements the calibration of the EDS system plays an important role. After measurement, taken data is compared with the reference peaks which is mostly provided by software on computer based X-ray spectrum analyzer (CXA) by using visual display KLM markers[58]. Not only rapid evaluation of the elemental constituents but also accurate analysis is provided by EDS.

3.4.1.6 Thickness Measurements

Thickness has an important role on the structural, optical and electrical properties of the films. For instance, the structure of the films whether they are amorphous or crystal likewise photon interactions whether they are transparent or opaque are the features that strongly dependent on the thickness. Therefore, determination of the film thicknesses is an important part of the characterization. In this study, thickness information of the films is obtained via by Veeco DEKTAK 6M profilometer working with computer control system with Dektak32 software. A diamond stylus with radius of 12.5 μm scanned the sample surface for a user defined distance while exerting user defined force. All measurements were done by taking substrate level as a reference point and obtain vertical profile of the films. In each deposition, 3 randomly picked samples were examined in order to obtain precise thickness values. Moreover, for collecting accurate results scan speed and scan length were controlled in measurements.

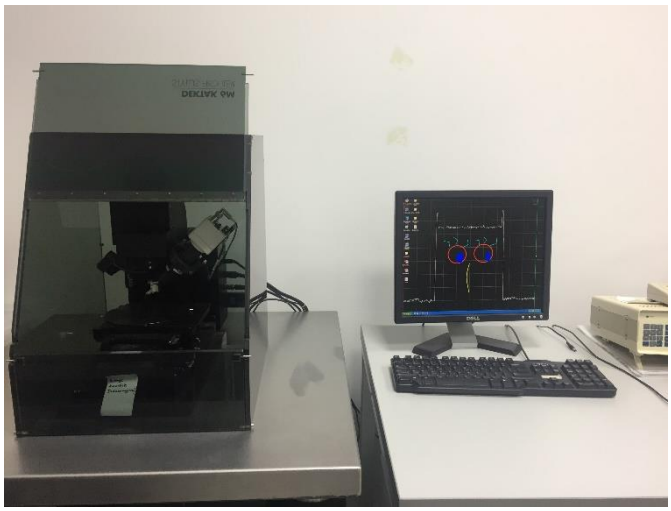

Figure 3-9. Dektak 6M profilometer

3.4.2 Electrical Analysis

3.4.2.1 Electrical Contacts

Metal contacts were made to examine the electrical and opto-electrical properties of the films. Different metals were used according to the films in order to provide the contacts showing the ohmic behavior where current and voltage show linear and symmetrical dependence. While Au was used as a contact material for CdTe and ternary $CdSe_xTe_{1-x}$ thin films, In was used for CdSe films in order to make ohmic contacts [1][2].

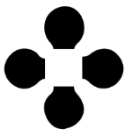

Figure 3-10. Metal contact mask

Metal contacts deposited as front contacts on the films by thermal evaporation. In order to obtain suitable contact geometry, copper masks that shown in Fig. 3.10 were employed.

Figure 3-11. Thermal evaporator for metal coating

Before deposition, copper metal contact masks attached to films and wrapped. Films were placed with substrate holder of thermal evaporation system shown in Fig. 3.11. Metal coating took place at approximately 10^{-6} Torr and at room temperature. Pure elemental metal (In or Au) was placed into tungsten boats which is heated by applying about 100V potential difference. As the evaporation of metal started, the shutter between substrate and source was opened. When metal coating was finished, shutter was closed, and voltage was decreased slowly. Sufficient amount of time was waited to break vacuum and samples were taken from thermal evaporation system. Since metal coating was done at room temperature, post heat treatment was applied to enable diffusion of the metals. Metal coated thin films were annealed at 100^{o}C for 30 min in horizontal Lindberg type furnace under constant nitrogen (N_2) gas flow. Electrical contacts were completed by Cu-wire connections. Copper wires were attached to films with the help of silver paste.

3.4.2.2 Current-Voltage (I-V) Measurements

Dark current-voltage (I-V) characteristic gives an important insight on electrical properties of the semiconductor thin films. In I-V measurements, user defined voltage difference is applied to samples and resulting current flow is measured. Measurements were carried out in dark to avoid possible photo-excitation of electrons which especially important for photosensitive materials such used in this study. To do so, in I-V measurements, thin film samples were placed inside metal box after probe wire connections were made. I-V measurements were carried out by using Keithley 2400 sourcemeter and LabVIEW computer program. The current-voltage measurement setup is shown in Fig. 3.12.

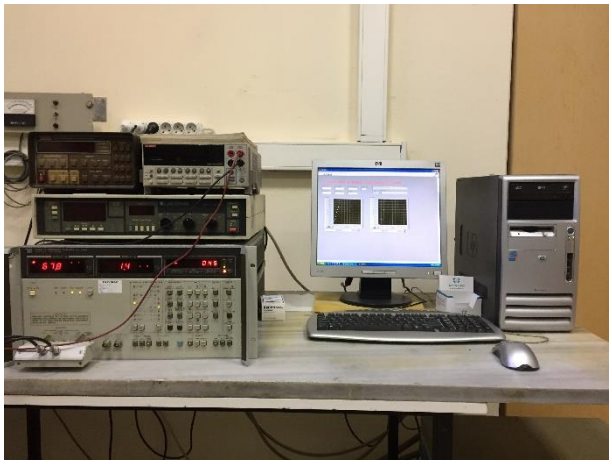

Figure 3-12. I-V measurement system

Applied voltage range was kept between -1V, +1V and resultant current was recorded. Voltage value was changed with 0.1 V steps and 1 second delay time was applied at each data taken.

3.4.3 Optical Analysis

3.4.3.1 UV-Vis Spectroscopy

UV-Vis spectroscopy is an efficient method to obtain optical properties such as transmissivity, reflectivity, absorption coefficient or optical band gap of thin films. In this method, photons having wavelength in ultraviolet and visible range is send to specimen and intensity of the transmitted photons is measured. The system provides an opportunity to analyze band gap value easily and rapidly while giving the spectral transmission behavior of the films. In this study, spectral transmission measurements were done by Perkin-Elmer LAMBDA 45 UV/VIS/NIR spectrometer as shown in Fig. 3.13. All samples were examined in the wavelength range between 350-1000 nm. In addition, background correction was done by subtraction of soda lime glass effect on transmission.

Figure 3-13. UV/VIS/NIR spectrometer

3.4.3.2 Photoconductivity

Photoconductivity measurements performed with Janis Liquid Nitrogen VPF Series Cryostat. With rotary pump attached to system photoconductivity measurements were done under $2x10^{-2}$ Pa. Moreover, temperature was controlled via liquid nitrogen cooling system. While analyzing temperature dependent photoconductivity behavior of the films, temperature range between 100-340 K was scanned with 10 K step. The temperature of the system was measured with GaAlAs diode sensor working with LakeShore 331 temperature controller. This system has 12 Watt halogen lamp placed at approximately 1 cm above samples to provide homogeneous illumination. Keithley 220 used as a current supplier of the lamp and operated between 50-90 mA with 10 mA increasing step for each data cycle. The corresponding illumination intensities with 50, 60, 70, 80, 90 mA current was obtained as 17, 34, 55, 81, 113 mW/cm^2 respectively.

For photoconductivity measurements films having van Der Pauw geometry was used. Samples were placed in cryostat and wire connections were made. Data taking process was started after reaching sufficient vacuum provided by rotary pump and setting desired temperature provided by addition of liquid nitrogen to the system. Constant bias voltage was applied by Keithley 2400 sourcemeter and resultant current values was recorded. The system was operated by LabVIEW computer program. Each cycle of data taking process started with measuring dark conductivity of the specimens in other words first data was taken without illumination at desired temperature. Afterwards, different illumination intensities included one by one and results was recorded. When the cycle was completed, the temperature of the system was increased with 10K step and the mentioned procedure was repeated.

CHAPTER 4

RESULTS AND DISCUSSIONS

4.1 Introduction

In this chapter, structural, optical and electrical characterization of $CdSe_xTe_{1-x}$ thin films were discussed with the experimental results. Firstly, structural analysis including composition and crystal structure of the films were presented. In this section, optimization of the post annealing process was discussed in detail. Secondly, band gap values and absorption behavior of the films was examined in optical characterization part. Lastly, electronic and optoelectronic properties of the films were explained with relevant results.

4.2 Structural and Compositional Analysis of $CdSe_xTe_{1-x}$ Thin Films

Six different deposition cycles were performed to investigate the effects of composition parameter, x, on the structural, optical and electrical properties of $CdSe_xTe_{1-x}$ thin films. The deposition parameters such as pressure, deposition rate was given in Chapter 2 and kept the same for all deposition processes.

4.2.1 EDX Analysis

The constituent elements of the films were analyzed by EDX system. Composition of the as deposited films in terms of atomic ratios is given in Table 4.1.

Table 4-1. Atomic ratios and average thickness (t_{avg}) values of as deposited $CdSe_xTe_{1-x}$ thin films

	Cd %	Te %	Se %	$\frac{Se}{(Se+Te)}$ %	t_{avg} (nm)
CdSe	50	-	50	-	300
$CdSe_{0.6}Te_{0.4}$	40	23	37	0.62	700
$CdSe_{0.5}Te_{0.5}$	40	29	31	0.52	700
T2-$CdSe_{0.3}Te_{0.7}$	45	38	17	0.31	800
T3-$CdSe_{0.3}Te_{0.7}$	48	35	17	0.33	600
CdTe	38	62	-	-	400

According to EDX results of the as deposited films, the composition parameter was calculated and found as x=1, 0.6, 0.5, 0.3, 0. In addition, approximate thickness values of the films shown in Table 4.1 were obtained by averaging three different sample thickness measurements. As mentioned in deposition section in Chapter 2, stacking layers were changed with the deposition thickness of CdTe and CdSe in order to change composition. There are two depositions which share the same composition parameter, x=0.3, this caused by some technical problem about thickness monitor. Since thickness could not be controlled precisely during the deposition, these two films resulted in the same stoichiometry.

The effect of post annealing process to the composition was analyzed according to varying annealing time and temperatures. CdSe, CdTe and $CdSe_{0.6}Te_{0.4}$ thin films annealed at 200, 300 and 400℃ for 30 minutes as a starting point. The improvement on crystallinity of the films at higher annealing temperatures, which is explained in detail in following sections, was observed. Due to improvement, in following deposition, $CdSe_{0.5}Te_{0.5}$ films were annealed at 450℃ for 30 minutes. However, these annealing conditions caused uncontrolled variations in the composition. The atomic ratios of constituents for sample annealed at 450℃ were found as Cd: 47%, Te: 33%, Se: 20%. These results indicate that the composition parameter x=0.5 for as grown sample were changed to x=0.3 after post annealing procedure. The decrease in Se ratios can be explained by relatively low melting point of Se when compared to Cd and Te[60]. Moreover, sticking coefficients plays an important role on deposition of the films with desired composition. In $CdSe_xTe_{1-x}$ structure, Se have the lowest

sticking coefficient; hence, escaping or segregation of Se atoms occurs at high annealing temperatures[60]. Therefore, it was observed that annealing temperatures above 400℃ leads to re-evaporation of Se uncontrollably which resulted in undesired stoichiometry. For this reason, the time parameter of the annealing procedure was changed. By fixing upper temperature limit to 400℃, annealing time was increased to 60 minutes.

Table 4-2. Atomic ratios of $CdSe_xTe_{1-x}$ samples annealed at 400℃

	Cd %	**Te %**	**Se %**	$\frac{\mathbf{Se}}{(\mathbf{Se+Te})}$ **%**
CdSe	52	-	48	-
$CdSe_{0,6}Te_{0,4}$	42	25	33	0.57
$CdSe_{0,5}Te_{0,5}$	47	28	25	0.47
T2-$CdSe_{0,3}Te_{0,7}$	50	34	16	0.32
T3-$CdSe_{0,3}Te_{0,7}$	48	37	15	0.29
CdTe	40	60	-	-

The constituent elements of the films annealed at 400℃ are tabulated in Table 4.2. CdSe, CdTe, $CdSe_{0.6}Te_{0.4,}$ $CdSe_{0.5}Te_{0.5}$ films were annealed 30 minutes while T2 and T3- $CdSe_{0.3}Te_{0.7}$ films were annealed for 60 minutes. As seen from Table 4.2, the stoichiometry of the films remains intact up to annealing temperature at 400℃ for 60 mins. Hence, qualitative films can be produced in desired stoichiometry by applying one-hour post heat treatment for $CdSe_xTe_{1-x}$ ternary alloy.

4.2.2 XRD Analysis

X-ray diffraction measurements were performed with as-deposited and annealed films for each deposition. The effects of changing composition parameter and annealing conditions on crystal structure were analyzed by these XRD results.

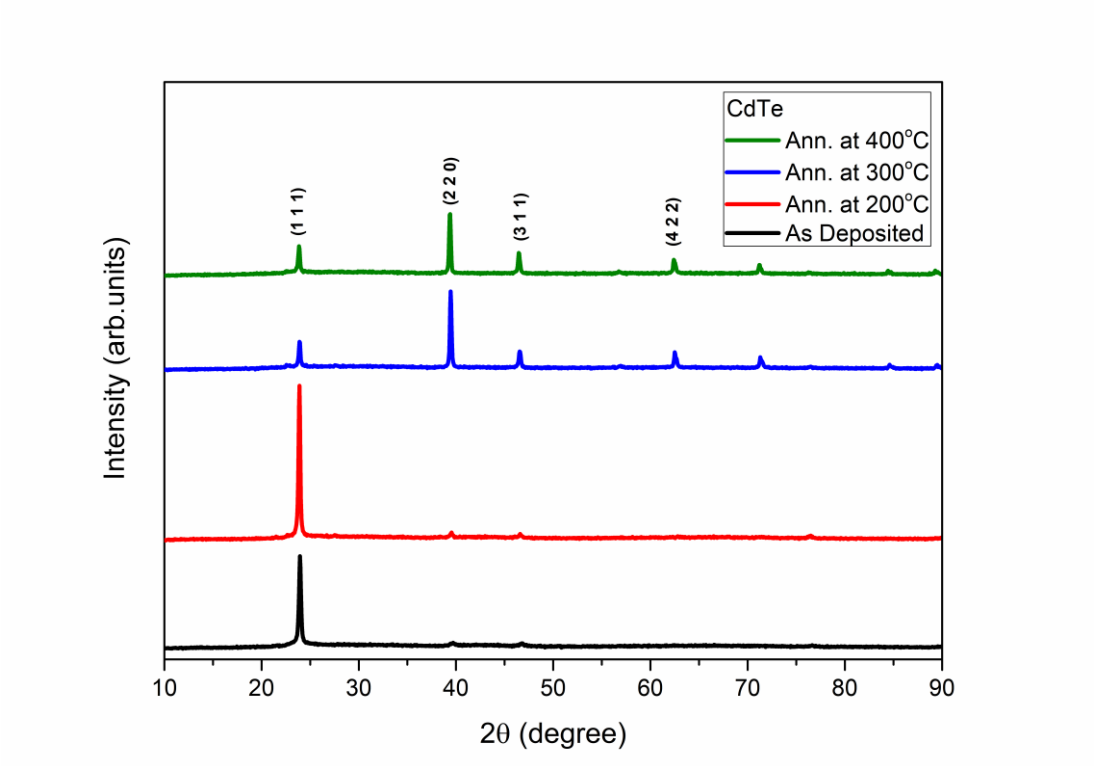

Figure 4-1. XRD results of CdTe thin films with varying post annealing temperatures

Characterization of CdTe as deposited thin films revealed that major peak is found at 23.9° which corresponds (111) cubic zinc-blend crystal structure confirmed by ICDD Card No:15-0770. Inter-planar distance, d, of the crystal structure was calculated by using Bragg's law and found as $d_{111} = 3.7$ Å and lattice parameter of the cubic structure was calculated by the formula,

$$\frac{1}{d_{hkl}^2} = (h^2 + k^2 + l^2)\frac{1}{a^2} \qquad (4.1)$$

where hkl are the miller indices, a is the lattice parameter and found as $a = 6.44$ Å. These results show high consistency with ICDD card information. Moreover, changings in crystal structure of CdTe with varying annealing temperatures is displayed in graph Fig 4.1. For the sample annealed at 200°C, the intensity of the (111) peak increased which implies improvement in crystallinity can be obtained by post annealing process. For CdTe samples annealed at 300°C and 400°C the shifting in the preferred orientation was observed. For these samples, diffraction peaks at 39.4°, 46.5°, 62.5°, 71.2°, which corresponds to (220), (311), (331), and (422) planes of cubic symmetry respectively, became dominant. The shifting in preferred orientation of CdTe thin films with post heat treatment is observed in the previous studies in literature and explained as the segregation of Te and reconstruction of the structure with vacancy distribution[9][61].

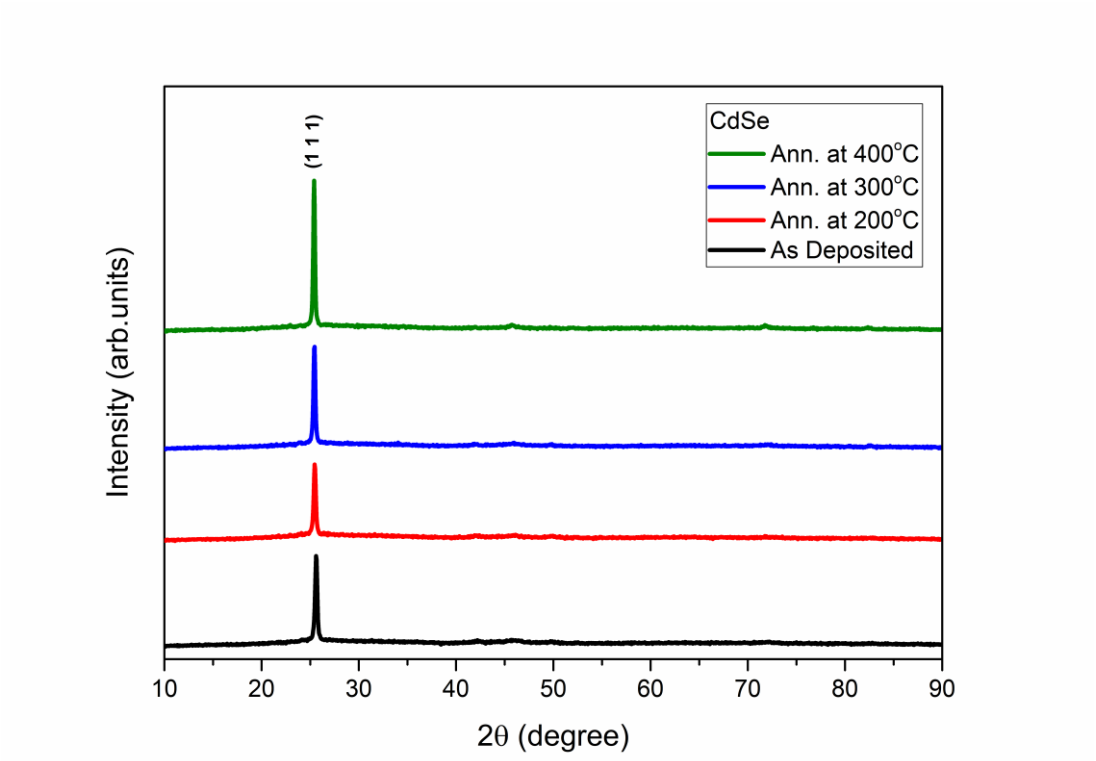

Figure 4-2. XRD results of CdSe thin films with varying post annealing temperatures

XRD results of CdSe thin films are presented in Fig. 4.2. XRD measurements of CdSe as deposited thin films revealed that major peak is found at 25.5° which corresponds

(111) cubic zinc-blend crystal structure confirmed by ICDD Card No: 19-0191. Inter-planar distance of the crystal structure was found as $d_{111} = 3.5$ Å with the help of Bragg's law and lattice parameter was calculated by Eq. 4.1 and found as $a = 6.06$ Å. These results are consistent with ICDD card information. It was found that with increasing annealing temperature the intensity of the peaks increases which implies that there is improvement in crystallinity.

Varying intensity values of XRD peaks of both CdTe and CdSe thin films confirm the polycrystalline nature of the films. Crystallite sizes were determined from X-ray diffraction measurements by using Scherrer's formula. Moreover, microstrain, ε, which is lattice strain originated from displacements of the atoms with respect to their ideal positions and dislocation density, δ, was calculated from XRD results. These results are summarized in Table 4.3.

Table 4-3. D, ε, δ values of CdTe and CdSe films with varying post annealing temperature

		D (nm)	**ε (x10^{-3})**	**δ (x10^{10} cm^{-2})**
CdTe	As Grown	29	5.86	11.8
	Ann. at 200°C	35	5.07	8.3
	Ann. at 300°C	35	5.05	8.3
	Ann. at 400°C	32	5.48	9.8
CdSe	As Grown	28	5.84	1.3
	Ann. at 200°C	28	5.86	1.3
	Ann. at 300°C	32	5.09	0.9
	Ann. at 400°C	36	4.54	0.8

In X-ray diffraction pattern of $CdSe_xTe_{1-x}$ films, mixture of CdTe and CdSe peaks were observed as shown in Fig. 4.3. All $CdSe_xTe_{1-x}$ as deposited films have diffraction peaks at 23.9° and 25.6° belonging to the CdTe and CdSe, respectively. Close relationship between composition and intensity of the peaks were observed. The intensity of the peak at 25.6° increased as the composition shifting towards to Se rich structure. For $CdSe_{0.6}Te_{0.4}$ thin films, the intensity of the peak belonging to CdSe was

slightly larger than CdTe peak, while in $CdSe_{0.5}Te_{0.5}$ XRD results the intensity of two peaks were nearly the same. As ternary films become Te rich, the CdTe peak at 23.9^0 became more intense.

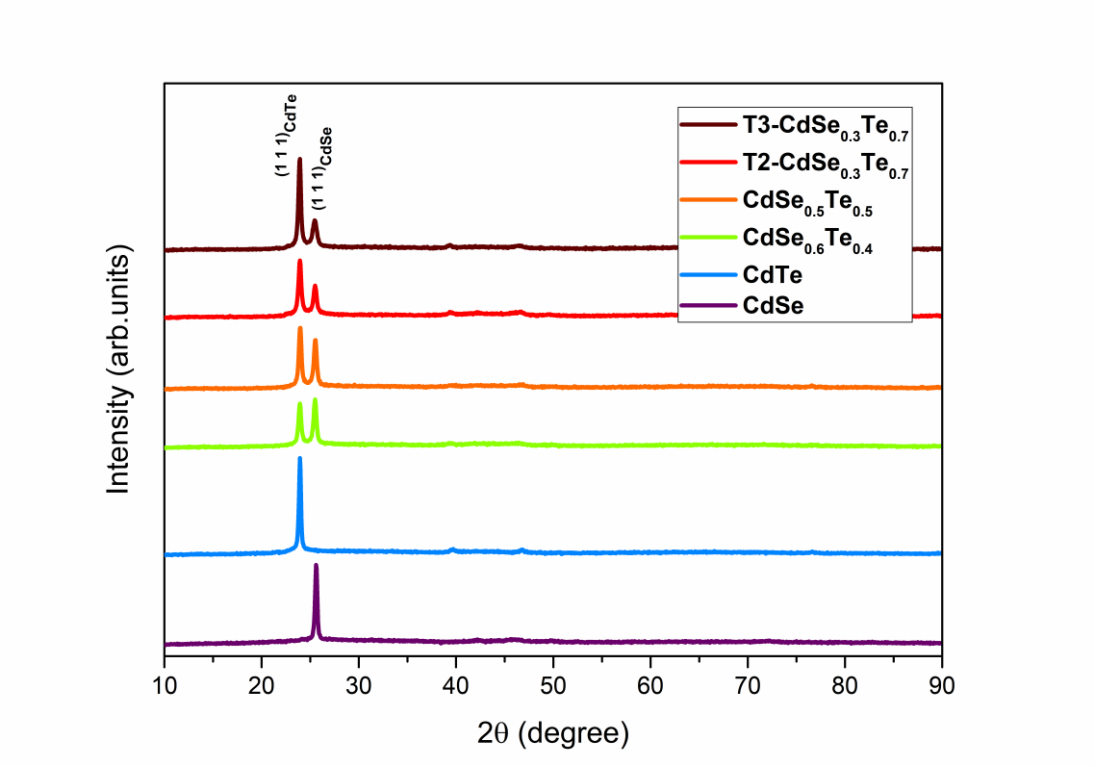

Figure 4-3. XRD results of as deposited $CdSe_xTe_{1-x}$ thin films

The X-ray diffraction results of ternary $CdSe_xTe_{1-x}$ revealed that crystal structure depend on post heat treatment. In analysis of post annealing effects on structure of $CdSe_xTe_{1-x}$ films, the shifting of the peaks was observed for different annealing temperatures. Regardless from composition, it was found that CdTe and CdSe peaks approached to each other for all deposited ternary alloys with increasing in annealing temperature. Since changing in preferred orientation was observed in CdTe films after post annealing, $CdSe_{0.3}Te_{0.7}$ was chosen as a typical sample to display temperature dependent XRD results. By choosing Te rich ternary alloy as a typical sample, accurate analysis of phase changing behaviour of CdTe films in ternary alloy was observed. The dependence of X-ray pattern of $CdSe_{0.3}Te_{0.7}$ thin films to the post annealing temperature is presented in Fig. 4.4.

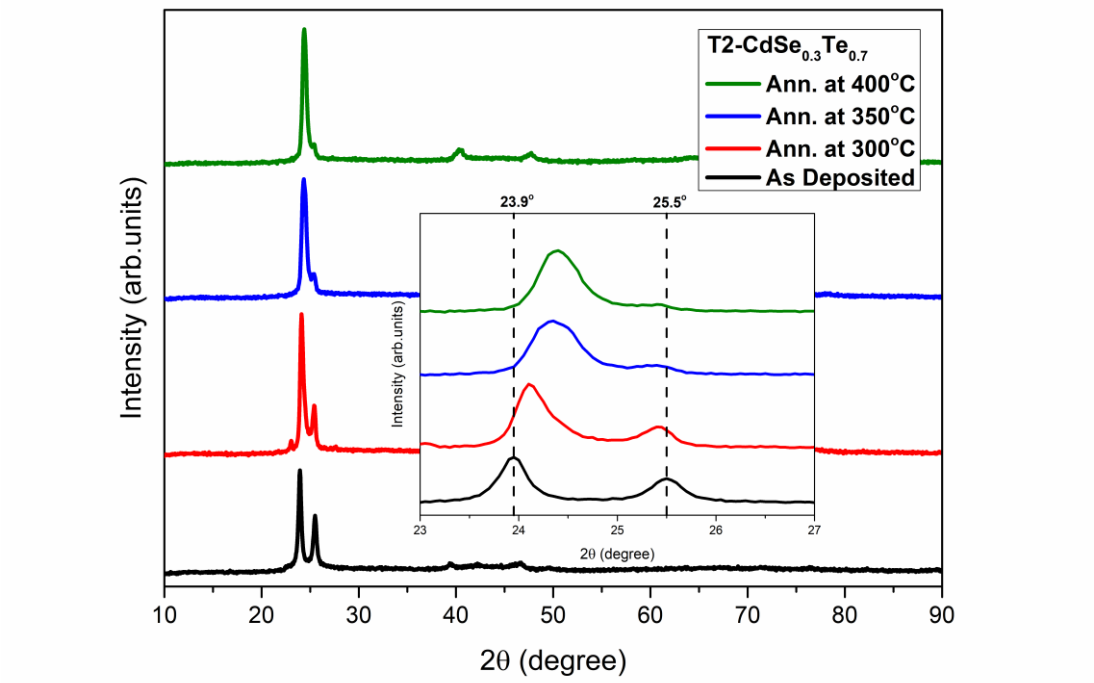

Figure 4-4. XRD results of $CdSe_{0.3}Te_{0.7}$ thin films with varying annealing temperatures

As the annealing temperature increases, it was found that independent peaks of CdTe and CdSe approached to each other. Shifting of the XRD peaks of $CdSe_xTe_{1-x}$ films is reported in literature with varying composition[62]. In this study, the sharp CdTe and CdSe peaks in XRD results for as deposited samples shifted and approached to each other with post heating. So that these shifting of the peaks can be interpreted as formation of ternary $CdSe_xTe_{1-x}$ structure with annealing, rather than having separate stacked layers of CdTe and CdSe. Results show agreement with the other studies reporting the peak splitting in $CdSe_xTe_{1-x}$ thin films[22]. Moreover, although the change in preferred orientation was observed for CdTe films after heat treatment at high temperatures, annealing at 300 and 400^0C of $CdSe_{0,3}Te_{0,7}$ films did not cause change in preferred orientation of CdTe layers in ternary thin films. These results may originate from the formation of stable structure in $CdSe_{0.3}Te_{0.7}$.

4.2.3 Raman Spectroscopy Analysis

Raman spectroscopy is an efficient tool to understand the nature of the vibrations in crystals, stress and strain of the structures. Composition effects on Raman spectroscopy results were identify by examining $CdSe_xTe_{1-x}$ films, while post heat treatment effects were analyzed in every deposition itself.

There are two Raman peaks of CdTe are observed at 140 and 168 cm^{-1} corresponding to transverse and longitudinal phonon modes respectively[45]. While as deposited CdTe films have one broad peak including these two modes, the peak splitting occurs with annealing process. This result may indicate that the orientation of the films is improved by post annealing procedure. Additional thermal energy may separate two different vibrational sources and leads to formation of two separate Raman peaks. For CdTe samples annealed at 200 and 300°C, one additional peak at 122cm^{-1} corresponding to Te phonons appears in Raman spectrum[45]. By annealing, Te vibrational states became more dominant and detectible in Raman spectroscopy. For the sample annealed at 400°C the intensity of all the peaks decreased relative to the other samples. This can be interpreted as decreasing symmetry in crystal structure especially when considering with the decrease intensity of the XRD peak of the same sample.

On the other hand, in Raman spectrum of CdSe films two peaks at 208 and 417 cm^{-1} were observed and confirmed as the first and second order longitudinal optical modes[63][64][46]. Having broad peaks rather than sharp peaks in CdSe Raman spectra, could be explained by poor crystallinity and defective structure of these thin films. Due to shifting of atoms with respect to their original positions, vibration sources of the material were spread, and hence, leads to formation of broad Raman peaks. Furthermore, any significant change did not occur with different post heat treatment procedure on both position and intensity of CdSe Raman peaks.

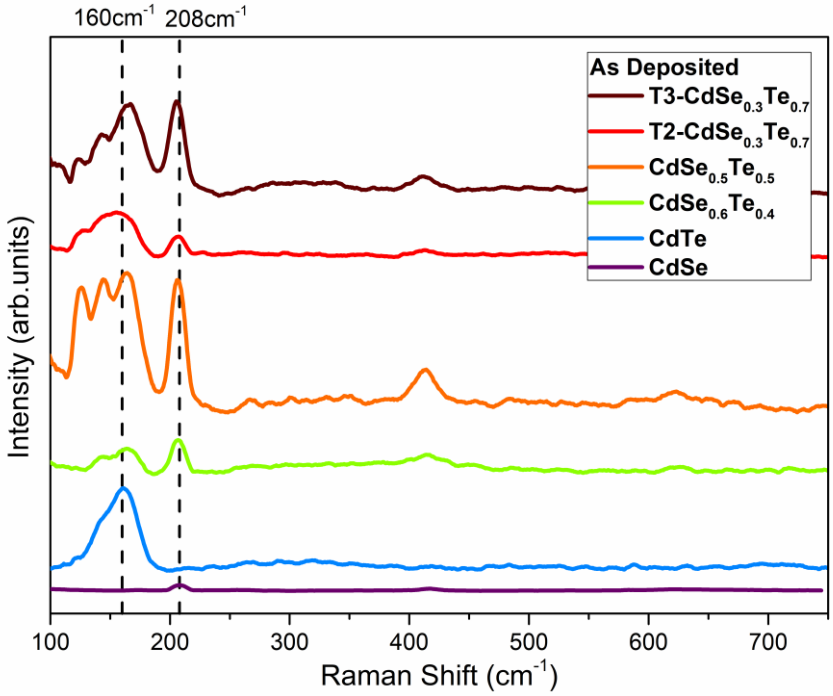

Figure 4-5. Raman spectra of as deposited $CdSe_xTe_{1-x}$ thin films

Raman spectra of as deposited $CdSe_xTe_{1-x}$ films are displayed in Fig. 4.5. Similar to XRD results, Raman spectra of ternary $CdSe_xTe_{1-x}$ films include the combination of CdTe and CdSe Raman modes. Regardless from composition, peaks were observed at around 160 and 207 cm^{-1} in Raman spectra of all $CdSe_xTe_{1-x}$ films. Former might be attributed to CdTe vibrational modes and latter belongs to CdSe Raman modes. However, distribution of the Raman modes showed consistency with changing x value. In other words, CdTe related modes were stronger in Te rich $CdSe_xTe_{1-x}$ films while CdSe modes were more detectible in Se rich $CdSe_xTe_{1-x}$ thin films. In addition, in the results of as deposited $CdSe_xTe_{1-x}$ thin films, relatively small peaks at around 412 cm^{-1} were detected because of the contribution of CdSe layers in the ternary alloy. Although all $CdSe_xTe_{1-x}$ films showed similar trend in Raman spectra, there were peak splitting in $CdSe_{0.5}Te_{0.5}$ thin film. For the as deposited $CdSe_{0.5}Te_{0.5}$ thin films, Raman peaks were observed at 144, 163, 206 and 413 cm^{-1}. The first two are the contribution of CdTe layers while the last two belong to CdSe layers. Minor shifting of the modes

implied that there was inner stress occur which were expected as the structure modified from binary to ternary alloy. One additional peak at 126 cm^{-1} might belong to Te vibrational Raman mode ideally appearing at 122cm^{-1}[45]. This shifting of Te mode also attributed to inner stress of the structure.

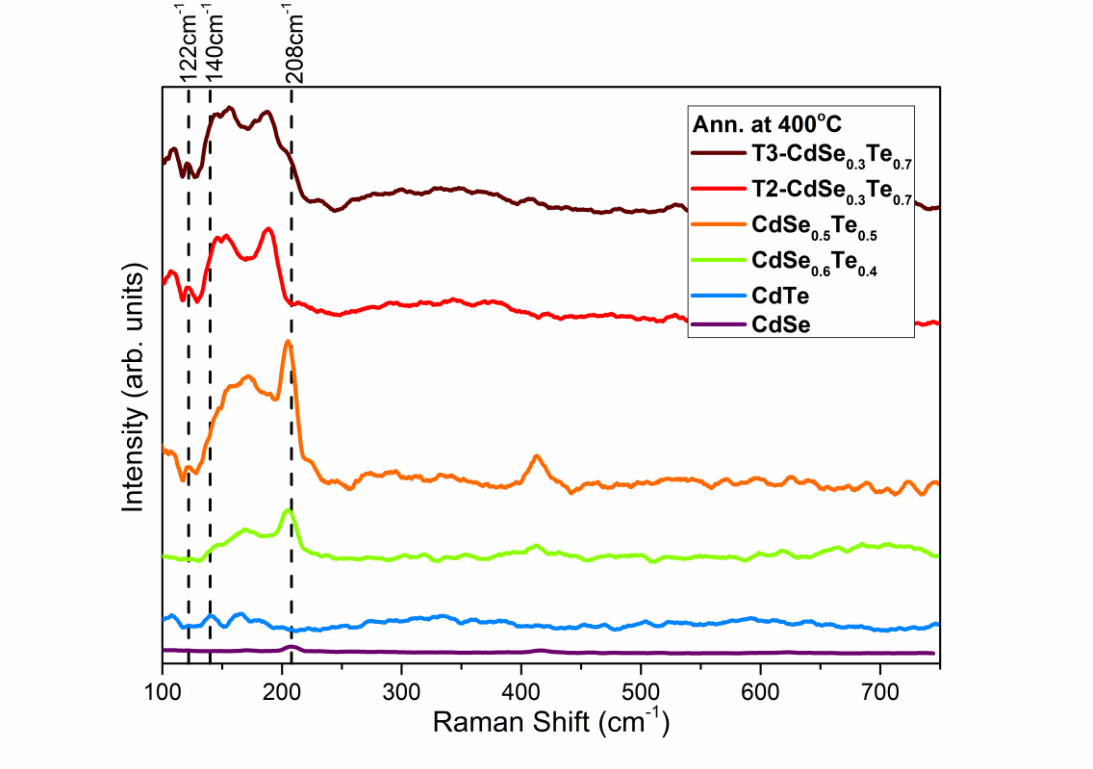

Figure 4-6. Raman spectra of $CdSe_xTe_{1-x}$ thin films annealed at 400 °C

The post annealing effects on Raman spectrum presented in Fig. 4.6. Raman spectrum showed similar trend with XRD results. As the annealing temperature increased the individual peaks of CdTe and CdSe approached. This result can be interpreted as, separate vibrational sources in the structure approached to each other and this was interpreted as interdiffusion of the layers.

4.2.4 AFM Analysis

Three-dimensional surface topographies of CdTe and CdSe films according to different annealing temperatures are given in Fig. 4.7 and Fig. 4.8. As can be seen from AFM surface images small roughness values were observed.

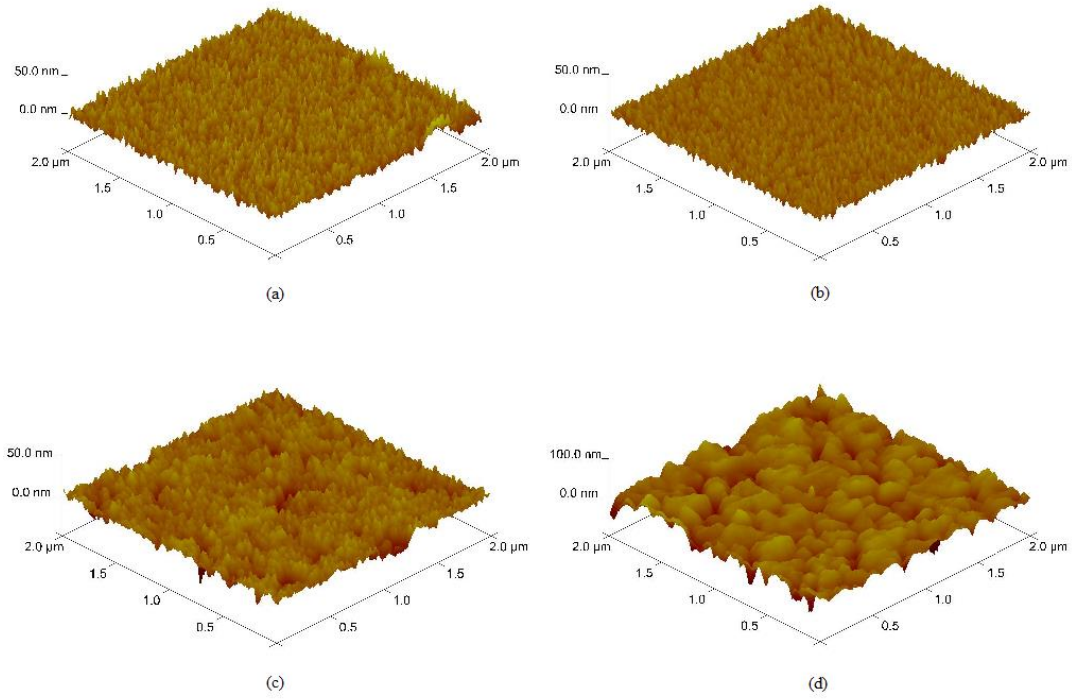

Figure 4-7. 3D AFM images of CdTe thin films, (a) as deposited, and annealed at (b) 200°C, (c)300°C, (d) 400°C

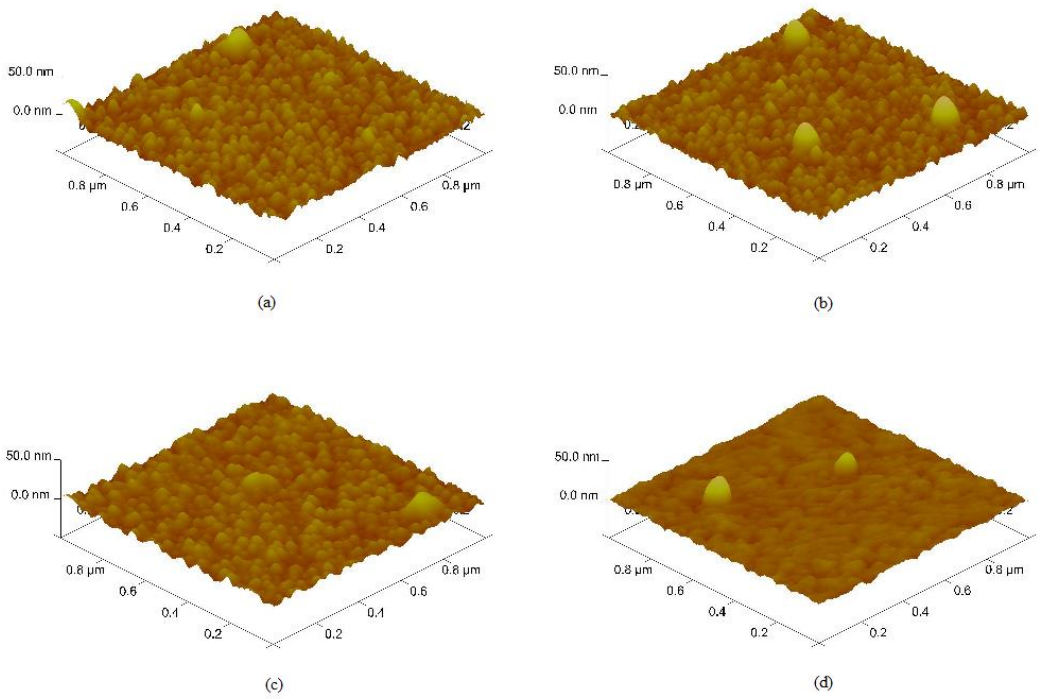

Figure 4-8. 3D AFM images of CdSe thin films, (a) as deposited, and annealed at (b) 200°C, (c) 300°C, (d) 400°C

Table 4-4. Average surface roughness (R_a) values for CdTe and CdSe thin films

	Samples	**R_a (nm)**
CdTe	As Deposited	3.46
	Ann. at 200°C	2.94
	Ann. at 300°C	3.42
	Ann. at 400°C	8.41
CdSe	As Deposited	2.40
	Ann. at 200°C	1.97
	Ann. at 300°C	1.87
	Ann. at 400°C	1.34

The average roughness values of samples with varying annealing temperature are presented in Table 4.4. For CdSe thin films, increasing in annealing temperature caused decrease in average roughness of the films. On the contrary, there was no significant change with post annealing in the surface roughness values for CdTe samples up to temperature 400°C. CdTe sample annealed at 400°C has the largest roughness value.

The post heat treatment effect on $CdSe_{0.3}Te_{0.7}$ sample is given by given 3D AFM images of as grown and sample annealed at 400°C in Fig. 4.9. As can be seen, with annealing at high temperature small particles grew up and their particle sizes were in between 60-200 nm.

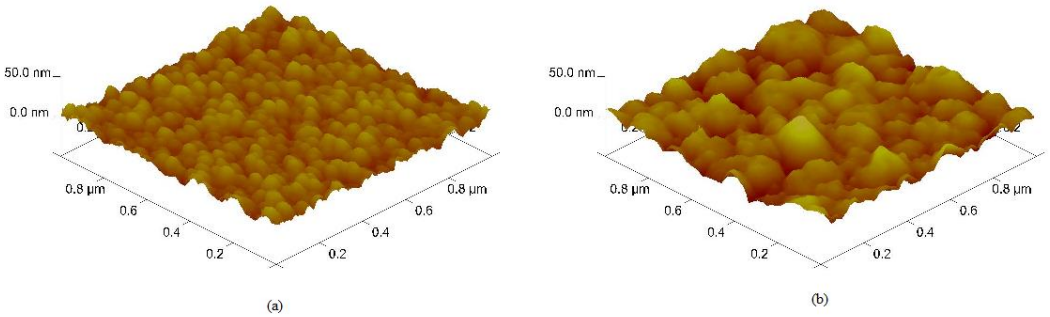

Figure 4-9. 3D AFM images of $CdSe_{0,3}Te_{0,7}$ thin films, (a) as deposited, (b) ann. at 400°C

The comparison of surface roughness values of $CdSe_xTe_{1-x}$ thin films was made between samples annealed at 400°C since the formation of ternary alloy was observed in these samples. The average surface roughness values are tabulated in Table 4.5.

Table 4-5. Average surface roughness (R_a) of $CdSe_xTe_{1-x}$ thin films annealed at 400°C

$CdSe_xTe_{1-x}$	**R_a (nm)**
$CdSe_{0,6}Te_{0,4}$	4.99
$CdSe_{0,5}Te_{0,5}$	4.65
T2-$CdSe_{0,3}Te_{0,7}$	6.25
T3-$CdSe_{0,3}Te_{0,7}$	4.32

In the overall AFM micrographs of the films, no cracks or holes were observed. This confirmed the post heat treatments did not cause any damaging effects on the surfaces of the films. In addition, homogenous distribution of the constituents was observed with AFM.

4.2.5 SEM Analysis

The surface properties of the $CdSe_xTe_{1-x}$ were examined by SEM. From the electron microscope images, it was observed that the films had a homogenous surface as observed from AFM results. Furthermore, no cracks were observed from the surface micrographs of ternary alloy.

The effect of post annealing process to CdTe films is given in Fig. 4.10. Although, as deposited and annealed at 200℃ samples have relatively flat surfaces, change in the surfaces occurred at the high annealing temperatures. As can be seen from micrographs of samples annealed at 300 and 400℃, the particle size enhanced with post heat treatment. Smaller particles became closer and the clusters with different sizes were formed after annealing at high temperatures. Furthermore, the dark points in SEM micrograph of the sample annealed at 400℃ shows pinholes which formed with post heat treatment. Since these holes are not observed for the as grown and annealed samples at 200℃, and they are observed for the samples at high annealing temperatures; it can be interpreted as a result of post annealing process.

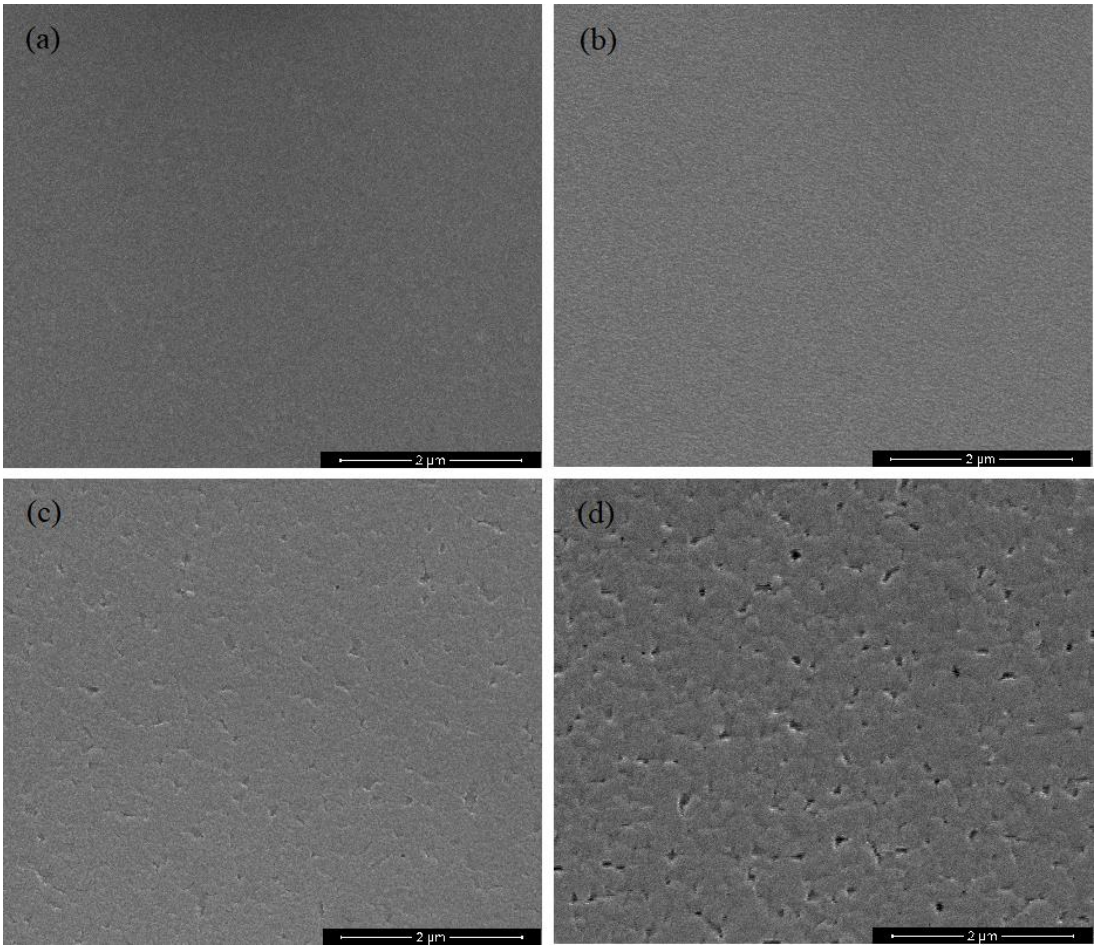

Figure 4-10. SEM micrographs of CdTe, (a) as deposited, and annealed at (b) 200 ℃, (c) 300 ℃, (d) 400 ℃

The SEM micrographs of the $CdSe_xTe_{1-x}$ are presented in Fig. 4.11 and Fig. 4.12. As deposited and samples annealed at 400℃ were compared to analyze the effects of post heat treatment. According to electron microscope images, films have flat surfaces with changing the particle sizes in between 20-100 nm. With annealing process at high temperatures, particles became apparent. These results are in good agreement with XRD results.

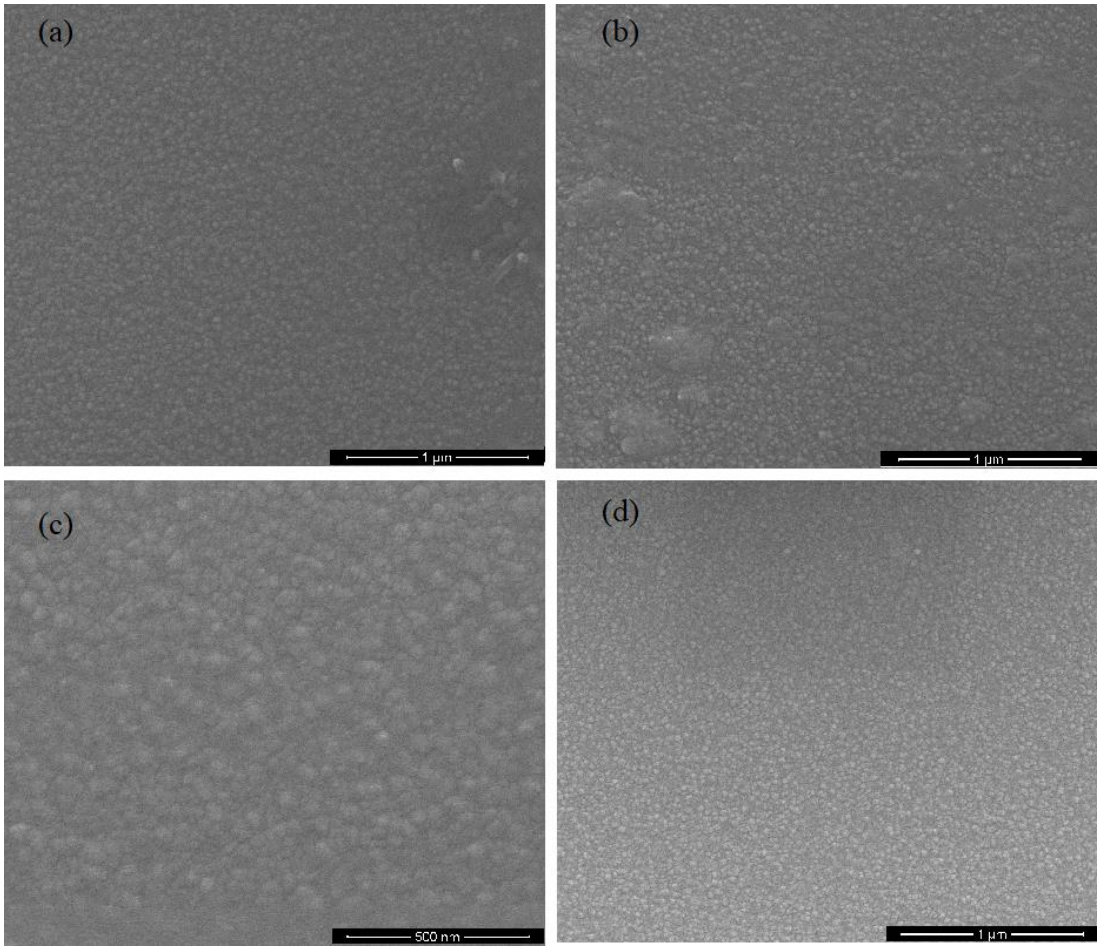

Figure 4-11. SEM micrographs of as deposited films, (a) $CdSe_{0,6}Te_{0,4}$, (b) $CdSe_{0,5}Te_{0,5}$, (c) T2- $CdSe_{0,3}Te_{0,7}$, (d)T3- $CdSe_{0,3}Te_{0,7}$

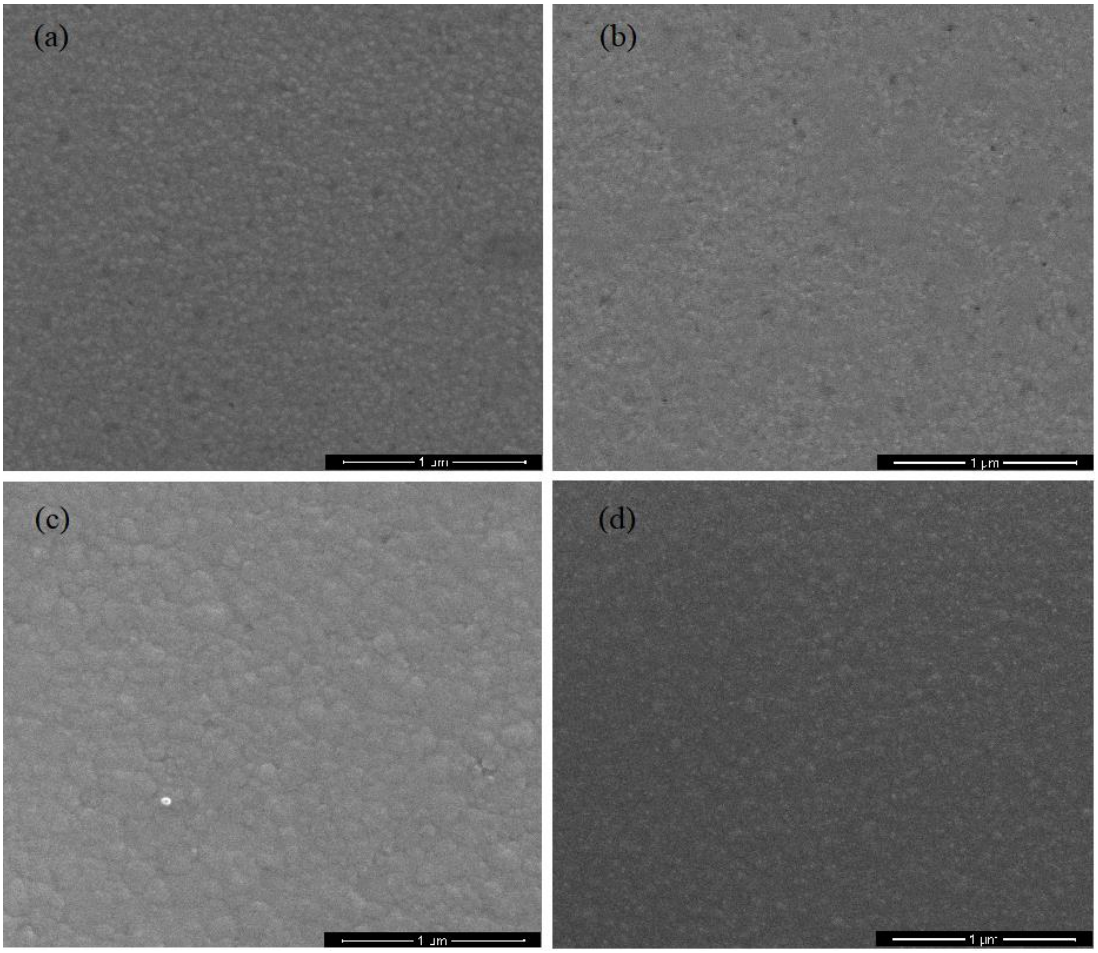

Figure 4-12. SEM micrographs of samples annealed at 400°C, (a) $CdSe_{0,6}Te_{0,4}$, (b) $CdSe_{0,5}Te_{0,5}$, (c) T2-$CdSe_{0,3}Te_{0,7}$, (d)T3- $CdSe_{0,3}Te_{0,7}$

4.3 Optical Analysis of $CdSe_xTe_{1-x}$ Thin Films

4.3.1 UV-Vis Spectroscopy Analysis

Transmission spectra and band gap values of the films are extracted from spectral transmission spectroscopy. Since reflection of the films were found negligible, absorption coefficient, α was calculated by Beer-Lambert law given in Eq. 2.8. Absorption coefficient in visible range for all films was calculated in the order of $10^4 cm^{-1}$ and no significant effect of post annealing on the absorption coefficient was

observed. Furthermore, the band gap values of the films were extracted from Tauc plots by applying linear fitting to the intersection points.

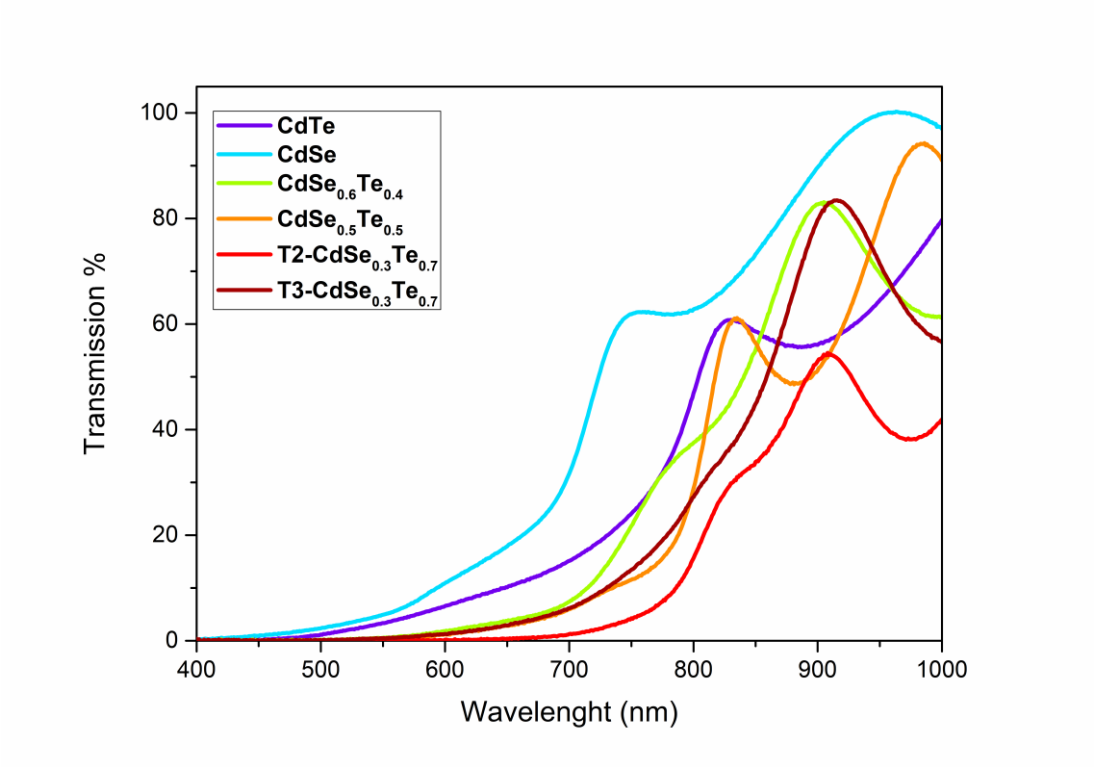

Figure 4-13. Transmission spectra of $CdSe_xTe_{1-x}$ thin films

Transmission spectra of $CdSe_xTe_{1-x}$ thin films are shown in Fig. 4.13. As can be seen from the figure, transmission spectra of $CdSe_xTe_{1-x}$ films shift towards to near infrared region with varying x parameter when compared to binary CdTe and CdSe films. This result indicates the transmission spectrum is strongly depending on composition parameter of $CdSe_xTe_{1-x}$ thin films. The same behavior was observed in the reported studies[23][26]. In Fig. 4.13, the transmission of T2-$CdSe_{0,3}Te_{0,7}$ is different and taking lower values in comparison with the other films. The underlying reason for this trend might be the thickness of T2-$CdSe_{0.3}Te_{0.7}$ films. As mentioned in previous sections, these films were thicker due to technical problem with thickness monitor.

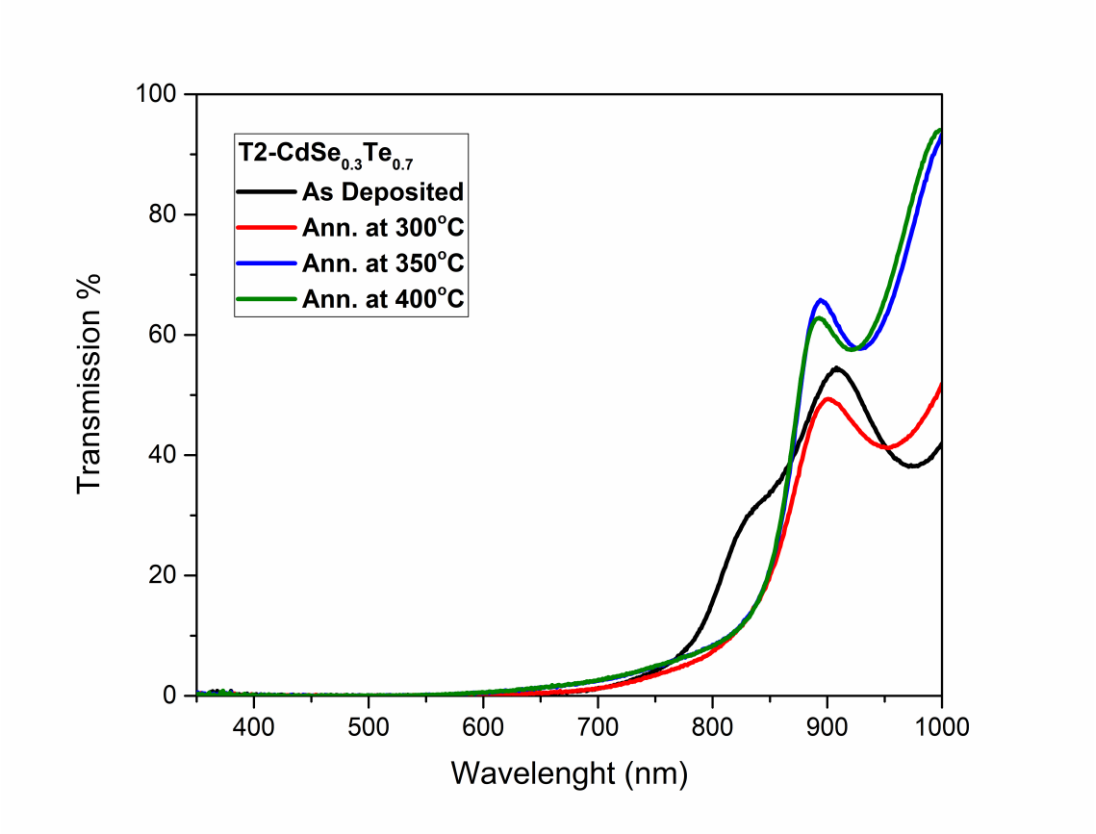

Figure 4-14. Transmission spectra of T2-$CdSe_{0,3}Te_{0,7}$ thin films with varying annealing temperatures

The band gap values were calculated by extrapolation of $(\alpha h\upsilon)^2$ vs $h\upsilon$ plots. The linearity of these plots showed that films have direct band gap. In addition, the effects of post heat treatment on the optical properties of the films were analyzed by transmission measurements. The transmission spectra and Tauc plots of T2-$CdSe_{0.3}Te_{0.7}$ thin films is presented in Fig. 4.14 and Fig. 4.15.

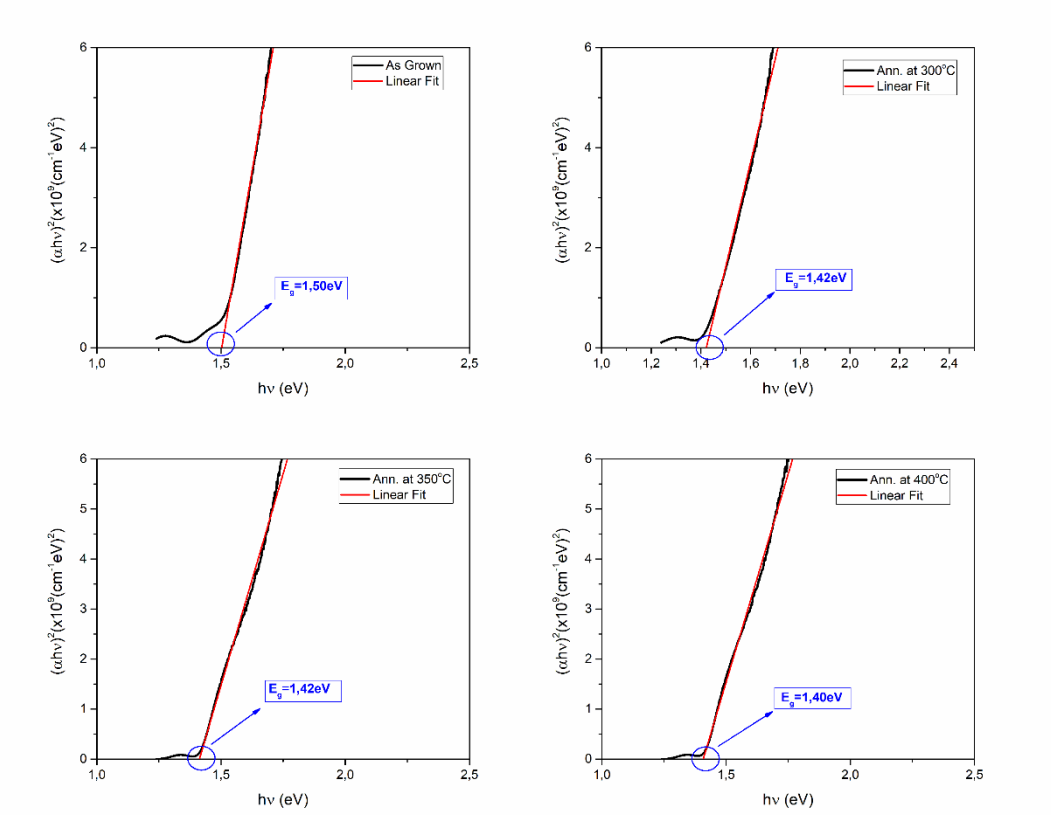

Figure 4-15. Tauc plots of T2-$CdSe_xTe_{1-x}$ samples with varying post annealing temperatures

Calculated band gap values of as deposited and annealed samples at 400℃ were summarized in Table 4.6. CdSe and CdTe films are having direct band gap values of 1.69 and 1.52 eV, respectively. The post annealing process does not cause significant changing on band gap values of both CdSe and CdTe films. The band gap of ternary alloys took values between CdSe and CdTe band energies for as grown samples. Unlike binary alloys, it was observed that the increasing post annealing temperature has more pronounced effect on the band gap energies of $CdSe_xTe_{1-x}$ thin films. As the annealing temperature is increased the band gap of $CdSe_xTe_{1-x}$ thin films decreased. Approximately 0.1eV decrease was observed in band gap energies of the samples annealed at 400^0C of $CdSe_xTe_{1-x}$ thin films. These results, with X-ray and Raman spectroscopy analysis, confirmed the formation of ternary alloy with post annealing

procedure. Hence, band gap tailoring was achieved by post heat treatment for ternary $CdSe_xTe_{1-x}$ films.

Table 4-6. Comparison of band gap values of $CdSe_xTe_{1-x}$ films between as deposited and samples annealed at 400°C

Samples	Band Gap Energy (eV)	
	As Deposited	Ann. at 400°C
CdSe	1.69	1.63
$CdSe_{0,6}Te_{0,4}$	1.60	1.60
$CdSe_{0,5}Te_{0,5}$	1.60	1.47
T2-$CdSe_{0,3}Te_{0,7}$	1.50	1.40
T3-$CdSe_{0,3}Te_{0,7}$	1.58	1.40
CdTe	1.51	1.48

4.4 Electrical Analysis of CdSexTe1-x Thin Films

Electrical properties were analyzed by using $CdSe_xTe_{1-x}$ thin films which were deposited in Van der Pauw geometry. The samples were deposited with suitable copper masks presented in Chapter 2, and the ohmic contacts were done by thermal evaporation of metal coating with the contact materials. Following to this metal coating, copper wire connection was done by soldering and silver paste. Electrical characterization of $CdSe_xTe_{1-x}$ thin films includes determination of the contact behavior and resistivity of the samples with I-V measurements. Moreover, temperature dependent behavior of conductivity both in dark and under illumination was studied in order to investigate electrical properties of $CdSe_xTe_{1-x}$ thin films.

By performing I-V measurements, the linear trend between current and voltage was observed. This linearity between current and voltage confirmed that an ohmic contact was formed between metal and $CdSe_xTe_{1-x}$ thin films. In temperature dependent photoconductivity measurements, the dark conductivity values of the samples were measured first, then samples were illuminated with different incident light intensities.

So that, dark resistivity of the samples at room temperature were calculated from photoconductivity measurements.

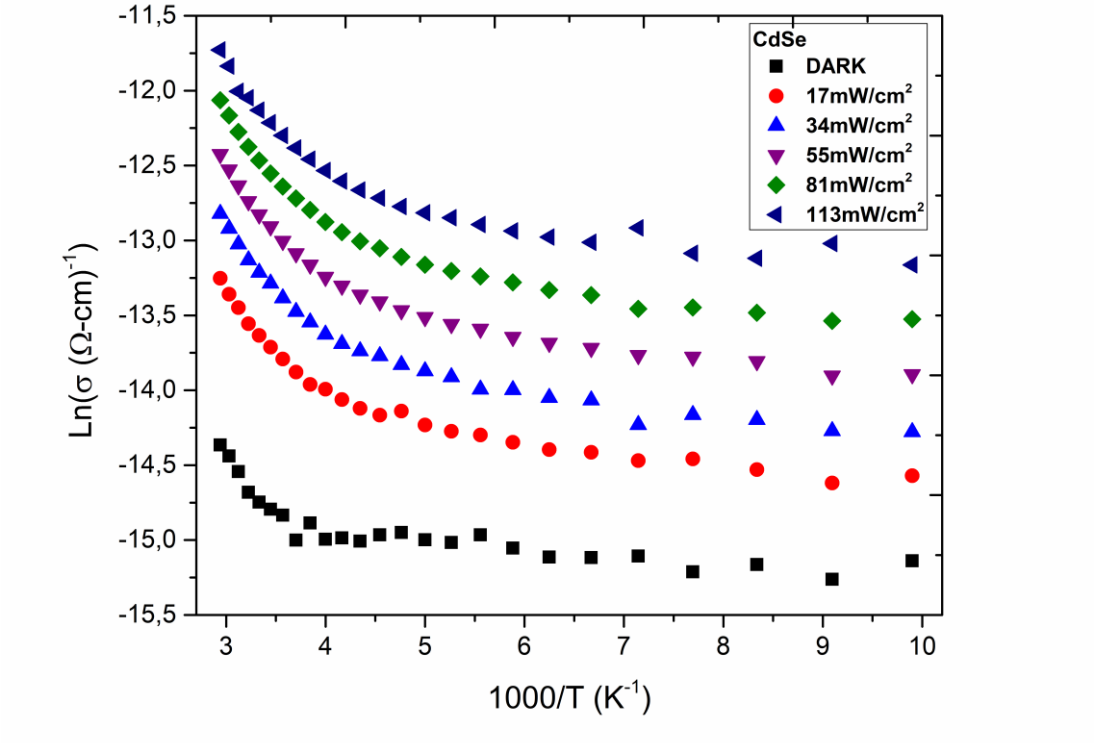

Figure 4-16. Photoconductivity results of CdSe thin films

It was observed that CdSe thin films had dark resistivity of 2.54×10^{6} (Ω.cm) and conductivity of $3.94 \times 10^{-7} (\Omega.cm)^{-1}$ at 300K. Temperature dependent conductivity results of CdSe thin films with varying photon intensities is shown in Fig. 4.16. As can be seen from the plot, CdSe thin films show their photoconductivity since conductivity values slightly changes with the incident photons. The trend of these changing differs between varying temperature regions in between 100 and 340K. The slope of the ln(σ) vs 1000/T plot took larger values for high temperature region, specifically between 270-340K. On the other hand, at lower temperatures the slope has smaller values. From these varying behaviors according to temperature, activation energy can be calculated by using Arrhenius expression, given in Eq. 2.20. The explicit fitting procedure for as deposited CdSe sample for temperature dependent

dark conductivity measurements is presented in Fig. 4.17. Activation energies were determined as E_{a1}=55.1meV between 270 and 340K and E_{a2}=3.44meV between 100 and 270K. These results indicate that CdSe thin films have smaller activation energies at low temperature region.

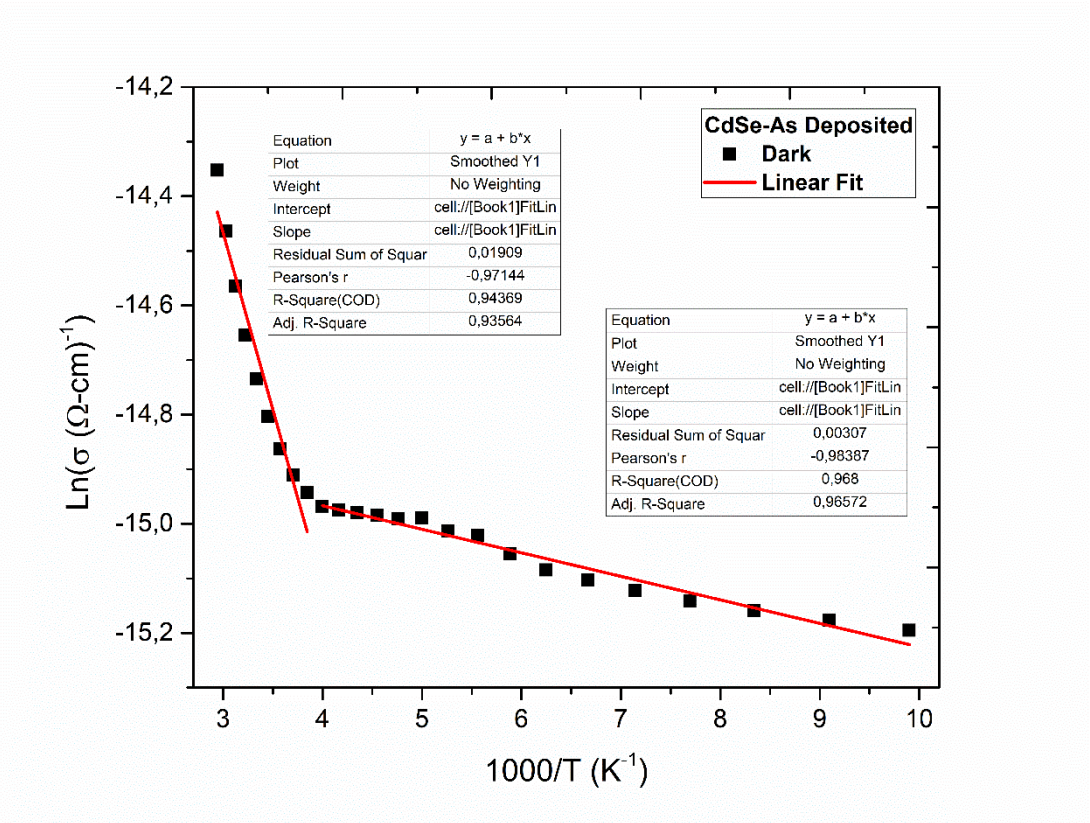

Figure 4-17. The dark photoconductivity variation of CdSe thin film; in between 100 and 340K

Electrical properties of CdTe thin films studied for the sample annealed at 400℃. Since at low temperatures, conductivity data cannot be taken for CdTe samples in photoconductivity measurements, these analyses were made in temperature interval 300-340K. The resistivity and conductivity of CdTe annealed at 400℃ were calculated as 4.13×10^{6}(Ω.cm) and 2.42×10^{-7}(Ω.cm)$^{-1}$ at room temperature, respectively.

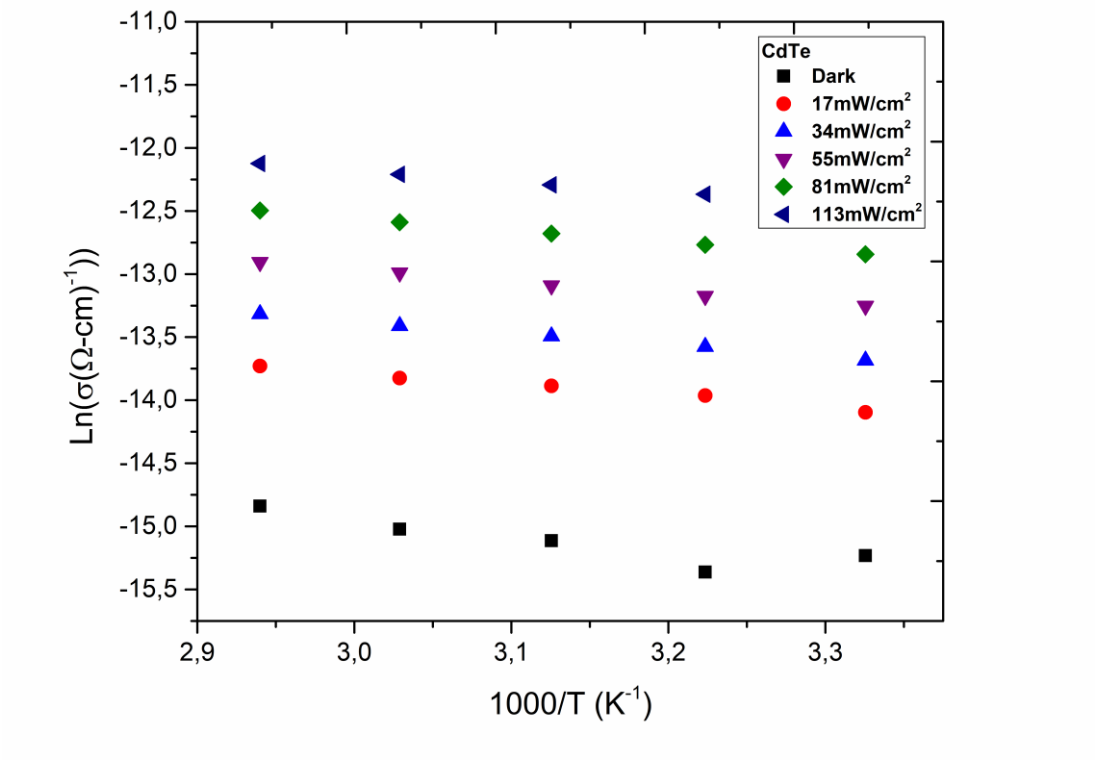

Figure 4-18. Photoconductivity results of CdTe thin films

As can be seen from ln(σ) vs 1000/T plot in Fig. 4.18, changes with external photon intensity can be attributed to conductivity orientation of CdTe film as a function of photon intensity. Since the temperature interval were limited and the trend of the line was not changed, activation energy of CdTe samples was determined for high temperature region as 99.9 meV for the samples annealed at 400^0C.

CdSe thin films showed extended conduction behavior when compared to CdTe thin films according to the temperature range. Because of this reason, Se rich ternary alloy, $CdSe_{0.6}Te_{0.4}$ thin films were chosen to investigate photoconductivity of $CdSe_xTe_{1-x}$ thin films. The ohmic behavior of the metal coated $CdSe_xTe_{1-x}$ thin films were observed via I-V measurements. The resistivity and conductivity of $CdSe_{0.6}Te_{0.4}$ were found as $1.95x10^6$ (Ω.cm) and $5.12x10^{-7}$ $(\Omega.cm)^{-1}$ respectively at room temperature. The resistivity of the ternary alloy is in the same order but slightly lower than the

resistivity of both CdTe and CdSe thin films. The photoconductivity results of $CdSe_{0.6}Te_{0.4}$ films are shown in Fig. 4.19.

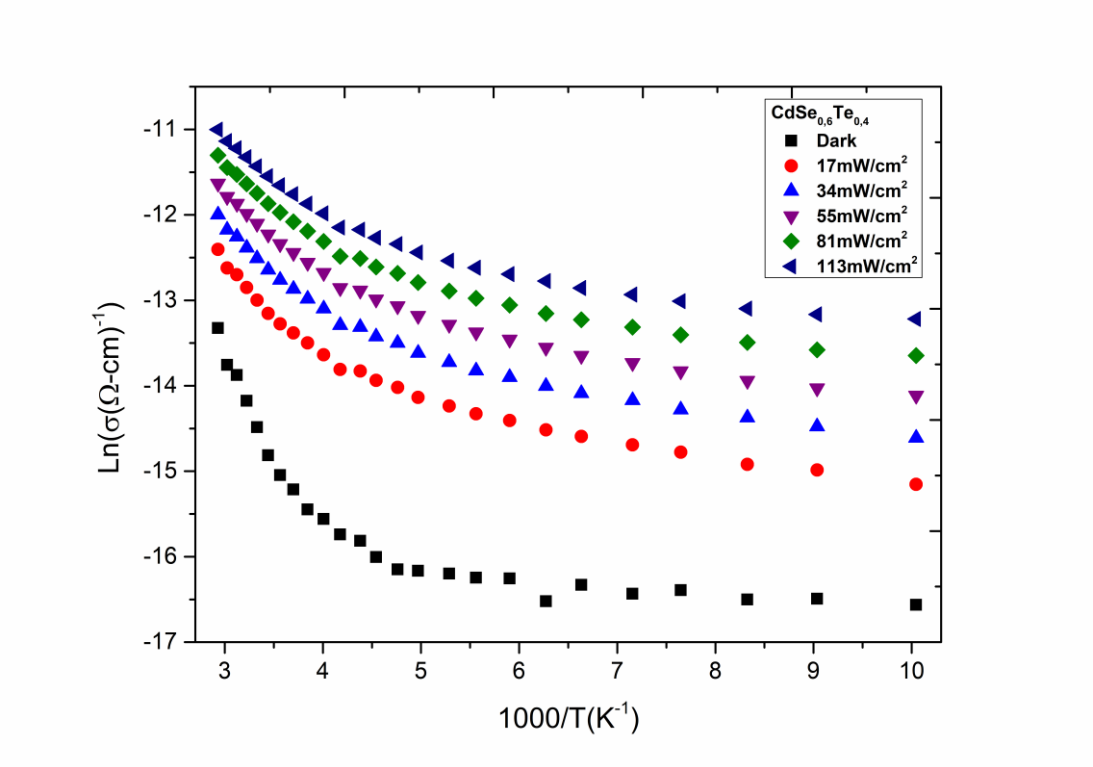

Figure 4-19 Photoconductivity results of $CdSe_{0,6}Te_{0,4}$ thin films

Similar to CdSe and CdTe, $CdSe_{0.6}Te_{0.4}$ films were found sensitive to external illumination. The activation energy calculations were made by considering as grown sample in dark as shown in Fig. 4.20. The behavior of ternary alloy is similar to CdSe thin films. In other words, unlike CdTe samples the photoconduction of $CdSe_xTe_{1-x}$ films could be investigated at low temperatures. The activation energies were calculated for $CdSe_{0.6}Te_{0.4}$ films in both hot and cold regions of the temperature interval. The activation energy of $CdSe_{0,6}Te_{0,4}$ thin films were 149.9 meV in between 250 and 340K and 7.76 meV in between 100 and 250K. Investigation of annealed $CdSe_xTe_{1-x}$ pointed that the post heat treatment procedure caused decrease in activation energies of the films. The calculated activation energies for $CdSe_{0.6}Te_{0.4}$ samples regarding post annealing temperatures are presented in Table 4.7. As the annealing temperature increased the activation energy of the sample decreased. This

result can be interpreted as the rearrangements via annealing resulted in well oriented structure and, hence, lower activation energies.

Table 4-7. The variation of activation energy with post annealing temperature for $CdSe_{0,6}Te_{0,4}$ thin films

$CdSe_{0,6}Te_{0,4}$	**E_{a1} (meV)**	**E_{a2} (meV)**
As deposited	149.9	5.17
Ann. at 300°C	123.2	0.43
Ann. at 400°C	91.3	3.44

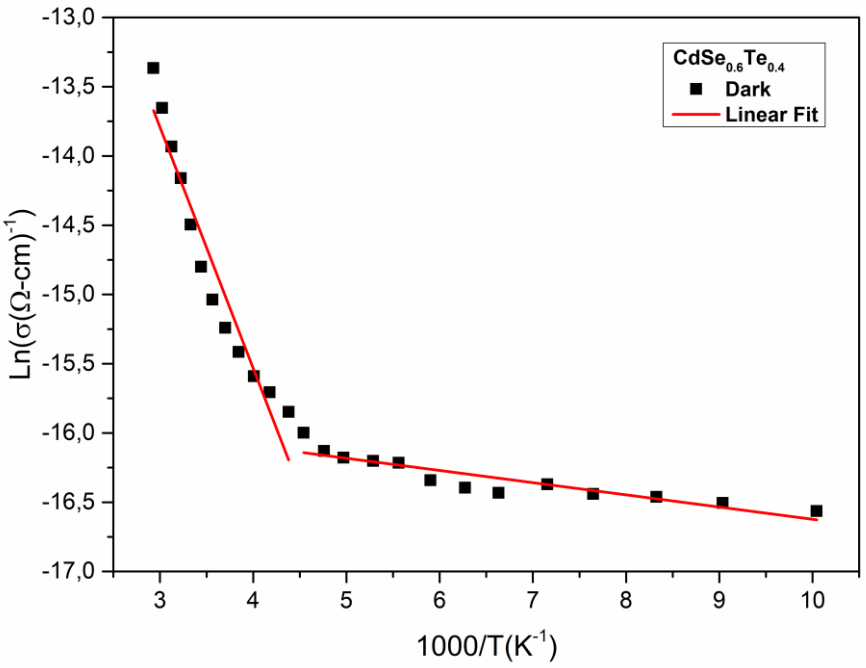

Figure 4-20. The dark photoconductivity variation of $CdSe_{0,6}Te_{0,4}$ film; in between 100 and 340K

CHAPTER 5

CONCLUSIONS

The main goal of this study was to produce $CdSe_xTe_{1-x}$ ternary alloy with varying stoichiometry and characterize the films by means of structure, optical and electrical behaviors. The optimized deposition parameters and effect of post deposition procedures, namely post annealing technique, was searched. Moreover, by employing wide spectrum of characterization methods, extensive analysis of the properties of $CdSe_xTe_{1-x}$ thin films was investigated. Besides optimization of deposition conditions, the effects of the composition on the structural, optical and electrical properties of the films was studied.

The $CdSe_xTe_{1-x}$ films were deposited by physical vapor deposition using two sources. CdTe and CdSe pellets were evaporated with e-beam and thermal evaporation methods, respectively. Thus, $CdSe_xTe_{1-x}$ films were synthesized by stacking CdTe and CdSe layers sequentially in the vacuum chamber which enable to use two evaporation techniques simultaneously. The composition parameter, x, was adjusted by variation of thickness of individual CdSe and CdTe layers. In each fabrication, layer thickness was changed in order to achieve desired stoichiometry while keeping the resultant film thickness the same. By this method, $CdSe_xTe_{1-x}$ films having close thickness values were deposited with different compositions.

The compositional analysis of the films was carried out via EDX measurements. According to EDX results, the composition parameter, x was found as 0, 0.6, 0.5, 0.3, 1. Therefore, characterization of $CdSe_xTe_{1-x}$ thin films was done in both Se and Te rich regions of the stoichiometry. Investigating the effects of the post heat treatment procedure on the properties of the $CdSe_xTe_{1-x}$ thin films were one of the main issues of this study. These effects were analyzed regarding changings on structural, optical and electrical properties of $CdSe_xTe_{1-x}$ films. Therefore, variation

in the stoichiometry with post annealing parameters such as temperature and process duration were investigated. The films having x value 0 ,1 and 0.6, which are CdSe, CdTe and $CdSe_{0.6}Te_{0.4}$, annealed at 200, 300 and 400°C for 30 minutes. The effects of the heat treatment with different temperatures was analyzed by making comparison with as deposited samples. It was observed that the crystallinity of the films improved as annealing temperature increased while no drastic changing occurred in composition. Therefore, $CdSe_{0.6}Te_{0.4}$ samples annealed at 450°C for 30 minutes. However, planned stoichiometry of the film was destroyed due to re-evaporation of Se. The composition changed uncontrollably by annealing at temperature 450°C. Therefore, the following step was to optimize the annealing duration after setting an upper limit of 400°C for temperature. The duration of post heat treatment was increased to 60 minutes. Moreover, since improvement was observed at high annealing temperatures, annealing at 200°C process was eliminated. Instead, in order to examine the post treatment effects in detail, 350°C annealing temperature was applied as a middle step. As a result, $CdSe_xTe_{1-x}$ films were annealed at 300, 350 and 400°C for 60 minutes. EDX results indicated that desired stoichiometry can be preserved while other properties of the films were improved by post annealing process up to 400°C for 60 min.

The structural properties of the films were analyzed by XRD and Raman spectroscopy measurements. The crystal structure and orientations were determined by XRD measurements. The analysis of CdTe as deposited thin films revealed that films have cubic zinc-blend structure in the direction of (111) plane. Similarly, XRD results of CdSe films showed that these films are also have cubic structure in (111) direction. The analysis of post annealing effects on XRD results showed similar trend for CdSe and CdTe thin films. The increasing intensities of the peaks indicate that the crystallinity was developed. In addition, while CdSe thin films preserved crystal orientation during heat treatment, shifting in preferred orientation was observed in CdTe films. At annealing above 200°C the preferred orientation of CdTe thin films shift from (111) to (220) direction with additional diffraction peaks. The variation of intensity of the XRD peaks proved that films have polycrystalline nature. The

remarkable results were obtained at XRD analysis of $CdSe_xTe_{1-x}$ thin films. In XRD results of ternary $CdSe_xTe_{1-x}$ as deposited samples, CdTe and CdSe XRD peaks were observed. Experiments exploited that there is a relationship between the intensity of the XRD peaks and the composition parameter. Furthermore, the investigation of annealing effects resulted in approaching of the separate peaks. As the annealing temperature increased the individual peaks of CdTe and CdSe films approach to each other which means inter-diffusion of the binary layers. Hence, the formation of ternary $CdSe_xTe_{1-x}$ films was observed by post annealing process.

The Raman spectroscopy analysis of the films were in accordance with XRD results. First, films have composition parameter x=0, 1 which are CdTe and CdSe, were investigated. Raman peaks were identified and confirmed in the light of information in literature. No significant effect of post heat treatment was observed at Raman spectra of CdSe thin films. However, peak splitting occurred at Raman spectra of CdTe films with increase in annealing temperatures. This can be interpreted as re-orientation of the structure with annealing. In addition, Te vibrational modes became more dominant in spectrum with post annealing procedure. Raman spectroscopy analysis of $CdSe_xTe_{1-x}$ thin films showed that peaks belong to CdTe and CdSe co-exist for as deposited samples. The significant results were obtained with post heat treatment. In Raman spectra of annealed samples, approaching of CdTe and CdSe Raman peaks was observed similar to XRD results. The formation of ternary alloy can be stated via these peak shifting. These results together indicate that deposition of $CdSe_xTe_{1-x}$ ternary alloy by stacking CdSe and CdTe layers is an effective method since formation of ternary alloy can be achieved by post heat treatment.

The surface structure of the films was examined by AFM and SEM. The average surface roughness of the films was low so that flat surfaces was observed in each deposition. Moreover, annealing did not show significant effect on surfaces. There were no cracks or holes was observed in both AFM and SEM results. The change in particle size due to annealing was examined and it is found that there was slight increment. Results showed that it is possible to improve quality of the $CdSe_xTe_{1-x}$ films by post heat treatment without damaging the surface or structure.

Optical characterization of $CdSe_xTe_{1-x}$ thin films was carried out by transmission spectroscopy in the wavelength range between 350-1000 nm. The shift in the transmission spectrum according to the composition of CdSexTe1-x thin films was obtained. $CdSe_xTe_{1-x}$ thin films spectra shifted towards to near infra-red region in comparison with CdTe and CdSe thin films. The absorption coefficient value was close for all depositions and found on the order of 10^4 cm^{-1} in the visible range. The nature of the band gap was extracted from Tauc plots. $CdSe_xTe_{1-x}$ thin films have direct band gap which taking different values according to composition of the films. Band gap values were found as 1.51 and 1.69 eV for CdTe and CdSe respectively. In fact, band gap of all ternary $CdSe_xTe_{1-x}$ alloys was found in between these two values for as deposited samples. However, critical variations were obtained in band gap of the films with post heat treatment procedure. Particularly for samples annealed at 400℃, a decrease in band gap of up to 1.40 eV was recorded. These variations in the band gap can be interpreted as the transformation from binary to ternary structure. In a similar manner with structural analysis, optical analysis exploit that with post heat treatment procedure, properties of $CdSe_xTe_{1-x}$ films can be manipulated.

Electrical analysis contained resistivity and photoconductivity measurements. The resistivity of the films was found of the order of 10^6 Ω-cm. In addition, linear trend was obtained in I-V measurements which implies the ohmic behavior of the metal semiconductor junction. In the temperature dependent photoconductivity measurements samples were illuminated with different intensities in the temperature range between 100-340K and hence, the activation energies were calculated. Firstly, CdSe and CdTe thin films were examined. CdSe samples showed photosensitive behavior in the whole temperature range, however, for CdTe films it was observed only in the region between 250-340K. Photoconductivity data of CdTe films in the cold region could not be taken due to resistivity problems. For ternary alloys, photo responsive behavior was observed in the whole temperature range. The post annealing process did not have significant effects on the electrical properties of the films.

In this study, ternary $CdSe_xTe_{1-x}$ thin films proposed as a qualitative candidate for solar cell applications with the tunable structural, optical and electrical properties. The deposition made by stacking CdSe and CdTe thin films provides control on the compositional parameter. With extensive analysis of post deposition treatments, particularly post annealing process it is shown that formation of ternary $CdSe_xTe_{1-x}$ thin films can be achieved. The post annealing procedure at 400°C for 60 min found as optimized conditions for formation of $CdSe_xTe_{1-x}$ high quality thin films.

REFERENCES

[1] C. Mitzithra, V. Kaniaris, S. Hamilakis, K. Kordatos, C. Kollia, and Z. Loizos, "Development and study of new hybrid semiconducting systems involving Cd chalcogenide thin films coated by a fullerene derivative," *Mater. Lett.*, vol. 65, no. 11, pp. 1651–1654, 2011.

[2] S. Mahato, N. Shakti, and A. K. Kar, "Annealing temperature dependent structural and optical properties of electrodeposited CdSe thin films," *Mater. Sci. Semicond. Process.*, vol. 39, pp. 742–747, 2015.

[3] C. Baban, G. I. Rusu, and P. Prepelita, "On the optical properties of polycrystalline CdSe thin films," *J. Optoelectron. Adv. Mater.*, vol. 7, no. 2, pp. 817–821, 2005.

[4] R. Manivannan and S. N. Victoria, "Preparation of chalcogenide thin films using electrodeposition method for solar cell applications – A review," *Sol. Energy*, vol. 173, no. August, pp. 1144–1157, 2018.

[5] S. Bera, S. B. Singh, and S. K. Ray, "Green route synthesis of high quality CdSe quantum dots for applications in light emitting devices," *J. Solid State Chem.*, vol. 189, pp. 75–79, May 2012.

[6] L. Guo *et al.*, "Improved stability and efficiency of CdSe/Sb2Se3 thin-film solar cells," *Sol. Energy*, vol. 188, no. January, pp. 586–592, 2019.

[7] J. Huerta-Ruelas, M. López-López, and O. Zelaya-Angel, "Molecular beam epitaxial growth of CdTe layers on InSb(111)A and B polar substrates," *Japanese J. Appl. Physics, Part 1 Regul. Pap. Short Notes Rev. Pap.*, 2000.

[8] T. D. Lee and A. U. Ebong, "A review of thin film solar cell technologies and challenges," *Renew. Sustain. Energy Rev.*, vol. 70, no. November 2016, pp. 1286–1297, 2017.

[9] T. M. Razykov *et al.*, "Characterization of CdTe thin films with different

compositions obtained by CMBD for thin film solar cells," *Sol. Energy*, vol. 144, pp. 411–416, 2017.

[10] E. R. Shaaban, N. Afify, and A. El-Taher, "Effect of film thickness on microstructure parameters and optical constants of CdTe thin films," *J. Alloys Compd.*, vol. 482, no. 1–2, pp. 400–404, 2009.

[11] R. Kulkarni *et al.*, "Structural and Optical Properties of CdTe Thin Films Deposited Using RF Magnetron Sputtering," *Energy Procedia*, vol. 110, no. December 2016, pp. 188–195, 2017.

[12] P. P. Hankare, K. C. Rathod, P. A. Chate, A. V. Jadhav, and I. S. Mulla, "Preparation and characterization of CuInSe2 thin films by chemical bath deposition technique," *J. Alloys Compd.*, vol. 500, no. 1, pp. 78–81, 2010.

[13] Himanshu, S. L. Patel, D. Agrawal, S. Chander, A. Thakur, and M. S. Dhaka, "Towards cost effective absorber layer to solar cells: Optimization of physical properties to Cu doped thin CdTe films," *Mater. Lett.*, vol. 254, pp. 141–144, 2019.

[14] G. Perna *et al.*, "Structural and optical characterization of Zn doped CdSe films," *Appl. Surf. Sci.*, vol. 233, no. 1–4, pp. 366–372, 2004.

[15] Ş. M. Huş and M. Parlak, "Electrical, photo-electrical, optical and structural properties of CdSe thin films deposited by thermal and e-beam techniques," *J. Phys. D. Appl. Phys.*, vol. 41, no. 3, 2008.

[16] S. L. Patel, Himanshu, S. Chander, M. D. Kannan, and M. S. Dhaka, "Effect of post-MgCl2 activation on physical properties of e-beam evaporated CdTe films for absorber layer applications," *Appl. Surf. Sci.*, vol. 498, no. July, 2019.

[17] M. A. Green, E. D. Dunlop, D. H. Levi, J. Hohl-Ebinger, M. Yoshita, and A. W. Y. Ho-Baillie, "Solar cell efficiency tables (version 54)," *Prog. Photovoltaics Res. Appl.*, vol. 27, no. 7, pp. 565–575, 2019.

[18] T. Baines *et al.*, “Incorporation of CdSe layers into CdTe thin film solar cells,” *Sol. Energy Mater. Sol. Cells*, vol. 180, no. March, pp. 196–204, 2018.

[19] B. B. Dumre, N. J. Szymanski, V. Adhikari, I. Khatri, D. Gall, and S. V. Khare, “Improved optoelectronic properties in CdSexTe1−x through controlled composition and short-range order,” *Sol. Energy*, vol. 194, no. November, pp. 742–750, 2019.

[20] X. Yang *et al.*, “Preparation and characterization of pulsed laser deposited a novel CdS/CdSe composite window layer for CdTe thin film solar cell,” *Appl. Surf. Sci.*, vol. 367, pp. 480–484, 2016.

[21] M. Lingg, A. Spescha, S. G. Haass, R. Carron, S. Buecheler, and A. N. Tiwari, “Structural and electronic properties of CdTe1-xSex films and their application in solar cells,” *Sci. Technol. Adv. Mater.*, vol. 19, no. 1, pp. 683–692, 2018.

[22] T. C. M. Santhosh, K. V. Bangera, and G. K. Shivakumar, “Synthesis and band gap tuning in CdSe(1-x)Te(x) thin films for solar cell applications,” *Sol. Energy*, vol. 153, pp. 343–347, 2017.

[23] N. Muthukumarasamy, S. Jayakumar, M. D. Kannan, and R. Balasundaraprabhu, “Structural phase change and optical band gap bowing in hot wall deposited CdSexTe1-x thin films,” *Sol. Energy*, vol. 83, no. 4, pp. 522–526, 2009.

[24] N. Matsumura, T. Sakamoto, and J. Saraie, “Growth conditions in molecular beam epitaxy for controlling CdSeTe-epilayer composition,” *MBE 2002 - 2002 12th Int. Conf. Mol. Beam Ep.*, vol. 251, pp. 383–384, 2002.

[25] S. K. Shinde, D. P. Dubal, G. S. Ghodake, and V. J. Fulari, “Synthesis and characterization of chemically deposited flower-like CdSe0.6Te0.4 thin films for solar cell application,” *Mater. Lett.*, vol. 126, pp. 17–19, 2014.

[26] A. Kathalingam, M. R. Kim, Y. S. Chae, J. K. Rhee, S. Thanikaikarasan, and T. Mahalingam, "Study on electrodeposited CdSexTe1-x semiconducting thin films," *J. Alloys Compd.*, vol. 505, no. 2, pp. 758–761, 2010.

[27] L. L. Berger, "Book : Semiconductor Materials," *CRC Press*, 1996.

[28] D. A. Neamen, *Semiconductor Physics and Devices Basic Principles*. 2006.

[29] Kittel C, *Introduction to Solid State Physics, 8th edition, Berkeley*. 1996.

[30] S. M. Sze and M. K. Lee, *Semiconductor Devices: Physics and Technology, 3rd Edition: Physics and Technology*. John Wiley & Sons, 2012.

[31] B. G. Streetman and S. Banerjee, *Solid State Electronic Devices*. Pearson Education Limited, 2015.

[32] D. K. Ferry and J. Bird, *Electronic Materials and Devices*. Academic Press, 2001.

[33] D. K. Schroder, *Semiconductor Material and Device Characterization: Third Edition*. 2005.

[34] D. A. Freser, *The Physics of Semi-Conductor Devices*. Oxford University Press, 1977.

[35] A. Elshabini *et al.*, *Thin Film Technology Handbook*. McGraw-Hill, 1998.

[36] L. T. Chu and S. S. Chu, "Thin Film II-VI Photovoltaics," *Solid State Electron.*, vol. 35, no. 3, pp. 533–549, 1994.

[37] S. Ikhmayies *et al.*, *Advances in the II-VI Compounds Suitable for Solar Cell Applications*. 2014.

[38] D. A. Barlow, "Predicting the temperature for the solid-solid phase transition in II-VI semiconductor alloys," *J. Phys. Chem. Solids*, vol. 74, no. 3, pp. 406–409, 2013.

[39] I. Hernández-Calderón, *Epitaxial growth of thin films and quantum*

structures of II-VI visible-bandgap semiconductors. 2013.

[40] X. Liang, D. M. King, and A. W. Weimer, "Ceramic ultra-thin coatings using atomic layer deposition," *Ceram. Nanocomposites*, pp. 257–283, 2013.

[41] J. Orava, T. Kohoutek, and T. Wagner, *Deposition techniques for chalcogenide thin films*. 2013.

[42] M. Tamargo, *II-VI Semiconductor Materials and Their Applications*. 2018.

[43] Z. C. Feng, M. J. Bevan, S. V. Krishnaswamy, and W. J. Choyke, "A photoluminescence comparison of CdTe thin films grown by molecular-beam epitaxy, metalorganic chemical vapor deposition, and sputtering in ultrahigh vacuum," *J. Appl. Phys.*, 1988.

[44] S. Lalitha, R. Sathyamoorthy, S. Senthilarasu, A. Subbarayan, and K. Natarajan, "Characterization of CdTe thin film - Dependence of structural and optical properties on temperature and thickness," *Sol. Energy Mater. Sol. Cells*, vol. 82, no. 1–2, pp. 187–199, 2004.

[45] J. Mitric *et al.*, "Surface optical phonon – Plasmon interaction in nanodimensional CdTe thin films," *Phys. E Low-Dimensional Syst. Nanostructures*, vol. 104, no. July, pp. 64–70, 2018.

[46] T. S. Shyju, S. Anandhi, R. Indirajith, and R. Gopalakrishnan, "Solvothermal synthesis, deposition and characterization of cadmium selenide (CdSe) thin films by thermal evaporation technique," *J. Cryst. Growth*, vol. 337, no. 1, pp. 38–45, 2011.

[47] A. Purohit, S. Chander, S. P. Nehra, and M. S. Dhaka, "Effect of air annealing on structural, optical, morphological and electrical properties of thermally evaporated CdSe thin films," *Phys. E Low-Dimensional Syst. Nanostructures*, vol. 69, pp. 342–348, 2015.

[48] J. D. Major, "Grain boundaries in CdTe thin film solar cells: A review," *Semicond. Sci. Technol.*, vol. 31, no. 9, 2016.

[49] G. M. Alonzo-Medina, A. González-González, J. L. Sacedón, and A. I. Oliva, "Understanding the thermal annealing process on metallic thin films," *IOP Conf. Ser. Mater. Sci. Eng.*, vol. 45, no. 1, 2013.

[50] B. D. Cullity, "Elements of X-ray diffraction, 2nd edition," *Addison-Wesley Publ. Co. Read. MA*, 1978.

[51] B. Ingham and M. F. Toney, *X-ray diffraction for characterizing metallic films*. 2013.

[52] P. F. Fewster, *X-Ray Scattering from Semiconductors*. 2003.

[53] J. R. Ferraro, K. Nakamoto, and C. W. Brown, *Introductory Raman Spectroscopy: Second Edition*. 2003.

[54] P. Vandenabeele, "Raman Instrumentation," in *Practical Raman Spectroscopy - An Introduction*, 2013.

[55] D. M. Haaland, "Vibrational spectroscopy, methods and applications A. Fadini and F.M. Schnepel, Ellis Horwood, Hemel Hempstead, 1989 (ISBN 0745800351)," *Anal. Chim. Acta*, 1990.

[56] R. W. Seizo Morita, Franz J. Giessibl, *Noncontact Atomic Force Microscopy volume 2*. 2009.

[57] B. Bhushan, "Nanotribology, nanomechanics and materials characterization," in *Nanotribology and Nanomechanics (Second Edition): An Introduction*, 2008.

[58] Goldstein Joseph *et al.*, *Scanning Electron Microscopy and X-ray Microanalysis*. 2003.

[59] R. F. Egerton, *Physical Principles of Electron Microscopy*. 2005.

[60] N. Muthukumarasamy, S. Velumani, R. Balasundaraprabhu, S. Jayakumar, and M. D. Kannan, "Fabrication and characterization of n-CdSe0.7Te0.3/p-CdSe0.15Te0.85 solar cell," *Vacuum*, vol. 84, no. 10, pp. 1216–1219, 2010.

[61] S. Chander, A. Purohit, C. Lal, and M. S. Dhaka, “Enhancement of optical and structural properties of vacuum evaporated CdTe thin films,” *Mater. Chem. Phys.*, vol. 185, pp. 202–209, 2017.

[62] D. E. Swanson, J. R. Sites, and W. S. Sampath, “Co-sublimation of CdSexTe1−x layers for CdTe solar cells,” *Sol. Energy Mater. Sol. Cells*, vol. 159, pp. 389–394, 2017.

[63] C. C. Bijumon and V. S. Kumar, “Raman PL And Hall Effect Studies Of Cdse Thin Film Deposited By Chemical Bath Deposition,” *Int. J. Sci. Technol. Res.*, vol. 4, no. 8, pp. 1–5, 2015.

[64] A. M. Kelley, Q. Dai, Z. J. Jiang, J. A. Baker, and D. F. Kelley, “Resonance Raman spectra of wurtzite and zincblende CdSe nanocrystals,” *Chem. Phys.*, vol. 422, pp. 272–276, 2013.